INSTITUTE
FOR
AEROSPACE STUDIES

UNIVERSITY OF TORONTO

VELOCITY MEASUREMENTS IN BUBBLY TWO-PHASE

FLOWS USING LASER DOPPLER ANEMOMETRY

(PART II)

by

W.E.R. Davies and J. I. Unger

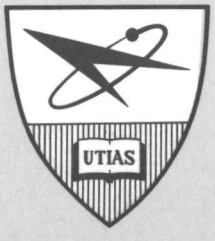

January, 1973.

UTIAS Technical Note No.185

VELOCITY MEASUREMENTS IN BUBBLY TWO-PHASE FLOWS USING LASER DOPPLER ANEMOMETRY (PART II)

by

W.E.R. Davies and J. I. Unger

Submitted December, 1972

January, 1973

UTIAS Technical Note 185

Acknowledgements

The authors wish to express their appreciation to Dr. I. I. Glass for his support throughout the work and for valuable criticisms during the preparation of the manuscript.

Dr. G. N. Patterson kindly made the facilities of the Institute available for this study.

Thanks are extended to Canaden Products (Montreal) for making a DISA frequency tracking available during part of the experiment and to Mr. D. D'Arcy of AECL for his assistance.

This project was supported financially through a contract from the Atomic Energy of Canada Limited (AECL).

Summary

The application of the laser Doppler velocity measuring technique to both turbid and bubbly flow media is described.

Two types of automatic frequency trackers have been tested and their performance evaluated under a variety of flow conditions.

A high frequency void fraction measuring instrument has been developed using a capacity principle and is used to provide information on flow conditions.

Full details on the electronics associated with the frequency tracking unit and the void fraction meter are included in the report.

TABLE OF CONTENTS

1. INTRODUCTION

A previous publication (Ref. 1) has described experiments, carried out at UTIAS, which demonstrated the feasibility of measuring the velocity of both phases (water and steam bubbles) in a bubbly two phase flow using laser-Doppler anemometry.

Further investigations, detailed in the present report, have been carried out and show that the technique can be applied to situations where the flow medium becomes quite turbid, and the void fraction is greater than 50%.

Instrumentation has been developed to enable continuous measurements to be made of the flow media velocities and also the instantaneous void fraction. In addition a commercially available frequency tracker has been employed to measure the velocity of the bubbly flows and its performance evaluated.

Full details of the electronic instrumentation, developed for this investigation are included in this report together with circuit diagrams and parts lists.

2. THE LASER DOPPLER TECHNIQUE

2.1 Laser-Doppler Anemometry

The Laser Doppler technique is currently used for velocity measurements in a great variety of flow problems. For many applications it is now used as a standard method, replacing many less contemporary techniques.

The advantages which the Doppler technique offers are as follows:

(i) No perturbation of the flow at the measuring point.

(ii) High spatial resolution.

(iii) It is absolute and linear, and is unaffected by the temperature of the medium being monitored.

These have prompted a few commercial enterprises to produce optical and electronic instrumentation to meet the requirements of many flow measuring problems.

While the specific problems associated with the measurements of coolant flow and velocities at AECL may preclude the direct application of the available equipment, the prospects seem bright for at least a partial automation of the measurement process.

2.2 Laser-Doppler Method

A description of the laser-Doppler method is contained in Ref. 1. However, for completeness a brief explanation of the process and formulation of the basic equations will be given here.

All laser-Doppler heterodyning processes rely on the formation of a real or virtual fringe pattern. This may be accomplished by the superposition of two beams, usually of equal intensity, derived from the same laser. In the case of small lasers ($\lesssim$ 30 cm cavity), path length differences of a few centimetres, between the laser output and the beam's intersection, do not seriously affect the fringe visibility. However, with larger cavities (such as in a 1 metre ion laser) care must be taken to equalize the path lengths for optimum fringe contrast (Ref. 2).

Figures 1a, 1b and 1c provide illustrations of the focussing geometry of the two beams derived from a laser, and will aid in the formulation of a few basic equations.

2.3 Fringe Spacing and Doppler-Modulation Frequency

Figure 1a shows the two equal intensity beams, of initial diameter d_o being focussed to a common region by the lens L_1. They are separated by a distance D before reaching the lens and intersect at an angle θ.

For simplicity we may consider each beam to have a Gaussian intensity distribution across its cross-section, and with plane wave-fronts represented by the hatched lines. At the focal point of the lens L_1 the wave fronts will intersect at the angle θ and an enlarged view of this region is presented in Figure 1b. Interference fringes will be formed throughout the focal volume. Bright fringes formed by the constructive addition of phase fronts are indicated by lines L_1, L_2 and L_3, while dark fringes are formed midway between these lines. Using the notation of the figure, the fringe spacing δ can be expressed as

$$\delta = \frac{\lambda}{2\sin\theta/2} \qquad (1)$$

If a particle traverses this fringe pattern and scatters light during its transit, such radiation can be monitored by a detector whose output would then be modulated depending on whether the particle is in a bright or dark portion of the fringe pattern. The frequency of this modulation is called the Doppler frequency f_D and it is related to the particle's velocity component (v), taken parallel to the Z axis, by the following expression:

$$f_D = \frac{2v\sin\theta/2}{\lambda} \qquad (2)$$

2.4 Focal Volume and Spatial Resolution

The size of the measurement volume formed by the intersection of the two beams is governed by the diameter of the beams at the focus and the intersection angle θ. Except for large beam separations (when 2 lenses should be used), spherical aberration is the only defect that warrants correcting in lens L_1. Good imaging quality is obtained by using a simple plano-convex lens and this should be mounted with the orientation shown in Figure 1a. At the focus of L_1 the diffraction limited diameter (d) of the focussed laser beam is given by:

$$d = \frac{4\lambda f}{\pi d_o} \qquad (3)$$

where d_o is the initial laser beam diameter and f is the focal length of lens L_1 at the laser wavelength λ (6328A for the He-Ne laser used in this experiment). The size d of the focussed beam given by Eq. 3 is the diameter of the $1/e^2$ intensity-ellipsoid which effectively contains the beams' intersection. In the X direction the minimum beam diameter is unchanged from that of d provided the beams are identical and overlap correctly; the other dimensions are obtained from and listed on the figure.

2.5 Number of Fringes

The total number of fringes within the $1/e^2$ intensity profile depends on the location along the Y axis. At Y=0 the number of fringes N in the XZ plane is simply $\Delta z/\delta$ and this can be shown to be:

$$N = \frac{2D}{\pi d_o} \qquad (4)$$

It is interesting to note that N is independent of the focal length of the lens L_1, depending only on the initial diameter of the laser beams d_o and their separation D.

For most automatic frequency trackers it is advantageous to have N large and this is therefore a quantity which should be optimized in conjunction with spatial resolution requirements. In addition, the accuracy of f_D, and hence the velocity, obtained from a single transit signal is directly proportional to N, a point which will be discussed later.

3. EXPERIMENTAL PROCEDURE

3.1 Extension of Previously Reported Experimental Work

Previous experiments carried out at UTIAS (Ref. 1) have shown that by proper optical procedures and appropriate signal handling, it is possible to discriminate between the scattering signals derived from bubbles or water in a two-phase bubbly flow. It was also shown that an optical system as sketched in Fig. 2 permits continuous velocity monitoring of both phases of the flow media.

Two equal intensity beams 1 and 2 from a Spectra Physics 1mw, He-Ne laser are focussed by lens L_1 to produce an intersection volume in the flow tube. Observation of the bubble velocity is made via a measurement of the Doppler frequency on detector 2, with detector 1 providing velocity information related only to the liquid flow.

One disadvantage of this arrangement is that only bubbles whose interfaces (closest to the incident light) intersect the focal volume will produce a Doppler signal. For some flows this may be unsatisfactory in that many bubbles will pass through the Y-axis with their velocities undetected. The length of the focal region could be increased to fill the width of the tube in the Y direction, providing Doppler signals for all interfaces crossing

this axis. However, such an arrangement makes simultaneous tracking along the Y axis difficult.

This particular problem may be circumvented by using the system shown in Fig. 3. The two equal intensity beams are focussed by L_1 into the tube, L_1 and D being selected so that angle Θ is sufficiently small to allow for overlap of the two beams throughout the tube diameter.

Light scattered by the bubbles into the X-direction is collected by the lens L_2 and focussed to form a real image of the laser-focus region, which can be scanned by a slit S before passing onto the detector. The position and width of S determines that portion of the Y-axis over which the velocity will be measured. Simultaneous monitoring of the whole velocity profile is also possible with a number of slits and companion detectors.

This side viewing method has another advantage. For example, by utilising a slit which accepts light from the whole of the length y_1y_2 and appropriate electrical frequency filters on the detector(s) output it is possible to track any chosen velocity (e.g. with a single detector and appropriate filter, it would be simple to check if a bubble had a velocity greater than some predetermined value, as set by the frequency filter).

3.2 Refractive Index Matched Viewing Cell

When viewing the Y-axis through a fluid filled tube as shown in Fig. 3 there is a lens effect (see Fig. 4). Light appearing to come from y_3 will actually have originated at y_4. This problem is serious with small diameter tubes and makes observations near the inner wall difficult.

This lens effect was eliminated in the present experiment by surrounding the tube with a water-filled chamber having parallel plates. There is then only a displacement error due to the tube wall. It can be shown using the notation of Fig. 4 that to a first approximation the displacement viewing error Δy, along the Y axis is:

$$\Delta y = \frac{yd}{R}\left[1 - \frac{\sqrt{R^2-y^2}}{\sqrt{k^2R^2-y^2}}\right] \qquad (5)$$

where

$$k = \frac{\mu_2}{\mu_1}$$

Good Doppler signals were obtained to within .010" of the tube wall using this technique.

3.3 Turbidity Due to Voids and Contaminants

3.3.1 Turbidity and Void Fraction

Questions were raised after the presentation of the original report (Ref. 1) concerning the viability of the laser-Doppler technique when operating with media where there is considerable turbidity or large average void fractions.

The variety of conditions that can be envisaged make this a difficult question to answer succinctly. Experiments, which will be described, show that the range of conditions over which the method continues to operate reliably is larger than was first anticipated.

3.3.2 Turbidity

This can arise either from the accumulation of small contaminant particles, or bubble concentrations of sufficient size and quantity to diffuse the incident light beams. The light in travelling through the flow medium will be attenuated and at some extinction level the coherence between the two beams will be reduced to the point where signal beating can no longer occur.

In Fig. 5 the fringe pattern at the focus is chosen to be just sufficient to give a useable Doppler signal. All that remains is for the scattered light to be transmitted through the liquid to the detector. It is apparant that the detection of the Doppler signal reduces to a case of observing a modulated light source at the focus. Thus only the thickness (t) of the flow medium that the incident light traverses in reaching the focus is of consequence.

It is possible that the loss of coherency decreases exponentially with path length, probably scaling as the attenuation due to turbidity.

$$I = I_o \, e^{-at} \qquad (6)$$

where

I = transmitted light after passing through thickness t.
I_o = incident light.
a = extinction coefficient due to scattering by the medium.
t = path length.

This has been observed qualitatively in our tests but it is difficult to be precise when visually evaluating the extinction level which corresponds to a loss of the Doppler modulation.

Whether heterodyning can be detected under any specific set of turbid conditions can certainly be determined by a test. However, some indication of the tolerance of the method may be gained from the results of a series of tests described below.

3.3.3 Experimental Turbidity Conditions

Bubbles Small bubbles (< 1mm dia) serve as very good light scattering and diffusing centres in a water flow. A continuous supply of bubbles, evenly distributed throughout the tube base was maintained using electrolysis. Currents up to 400 mA were passed through the water using the two electrodes shown in Fig. 3.

3.3.4 Contaminants

Both homogenised milk and tooth powder were used to simulate the effect of contaminants in the flow. Both of these substances disperse well in the water and could be added gradually with appropriate predilution.

3.3.5 Turbidity Results

A rough measure of the turbidity was provided by monitoring the transmitted level of an independent laser beam after passing through the flow tube. When the transmitted intensity had fallen to ~ 60% of that obtained with clear water, the Doppler signal was found to be inadequate for processing. This 60% level applied to both optical arrangements shown in Fig. 3, and for both bubble and contaminant induced turbidity.

3.4 Bubble Detector

In order to assess the limits over which the laser Doppler technique would operate reliably in a bubbly flow, it was necessary to measure the void fraction under a variety of bubble conditions and preferably in real time. To meet these requirements a bubble detector was constructed based on a capacity principle.

The dielectric constant (k) of water is fortuitously high [$k_{0°C} = 88$, $k_{100°C} = 48$, whereas $k_{AIR} \sim 1$] and the resulting capacity for a water-filled volume enclosed by two plates with a $1cm^2$ common area and placed 1cm apart is ~ 4×10^{-12} Farads at 100°C. Such capacities can readily be measured with a frequency response greater than 10 KHZ making it possible to detect air bubbles as small as 1mm diameter moving with water at flow velocities of 10^4cm/sec while traversing capacitor plates 1cm long.

For this experiment two thin copper plates approximately 1cm x 1.2cm were attached to the flow tube with epoxy, immediately below the optical observation region, Fig. 3. It can be shown for the plate arrangement outlined in Fig. 6, where a liquid of thickness d_3 and dielectric constant k_3 is contained in a parallel sided tube with walls of thickness d_2 and dielectric constant k_2, that the capacitance between the outer plates of common area A is given by:

$$C = \frac{A\varepsilon_o k_1 k_2 k_3}{2d_1 k_2 k_3 + 2d_2 k_1 k_3 + d_3 k_1 k_2} \text{ Farads} \qquad (7)$$

when MKS units are employed.

The distance d_1 is incurred when the plates are fastened to the tube's outer wall, k_1 is the constant for the filler medium or air, as the case may be.

In order to achieve the maximum sensitivity from the bubble detector, it can be shown by an evaluation of the above equation, that the plates should be as close to the tube wall as possible and the tube walls themselves should be as thin as practicable.

3.4.1 Calibration and Use of the Bubble Detector

A calibration curve for the bubble detector is shown in Fig. 7. This was obtained by varying the height of the water between the plates; this is a quick and simple procedure giving a nominal accuracy of ~ 5% at room temperature.

The change in capacity caused by voids passing between the plates was measured by instrumentation which will be described later in this report. It is the output of this electronic unit which is plotted as the ordinate in Fig. 7. Under flow conditions the instantaneous void fraction is conveniently monitored with an oscilloscope. Figures 8a and 8b are time traces of the bubble detector output when voids are produced by the introduction of high pressure air into the flow, and small bubbles are formed by electrolysis respectively.

3.5 The Effect of Voids on the Doppler Signal

3.5.1 Large Void Detection and Related Doppler Signals

In Fig. 8a the signal trace corresponds to a void fraction of approximately 50%, which at a flow velocity of 30 cm/sec indicates that individual pulses on the photo have originated from single bubbles of approximately 3mm dia traversing the plates' length (1.2cm). The longer pulses (~ 0.3 sec) would correspond to bubbles approximately 9cm long; these were not observed visually. However chains of bubbles about 10cm in length comprised of individual bubbles about 1cm in diameter were observed and these would account for the structure in the larger pulses and also the pulse length.

Good Doppler signals were obtained on both side and forward scattering detectors and the UTIAS frequency tracker was able to measure the velocity readily. Signals drop-outs (due to occlusion of the scattered radiation on detector 1) present no problem for the tracker since they have only low-frequency components and these are rejected by the input filter network.

3.5.2 Small Void Detection and Related Doppler Signals

In Fig. 8b the bubble detector output has been A.C.-coupled to the oscilloscope in order that the signal due to void fluctuations may be seen. The D.C. output in this case was 6mv corresponding to an average void fraction of ~ 1%. The width of the fastest pulse in this photograph is ~ 100msec and at a flow velocity of 22.5cm/sec the bubble detector output is responding to the change in the average total volume of small bubbles between the plates.

Good Doppler signals were obtained on both detectors for small-bubble void-fractions, up to the point. The UTIAS tracker behaved well up to the 1% void level but, rather disturbingly, continued to track at even higher void fractions even though the Doppler signal had disappeared (the same phenomenon was also observed with the commercial tracker).

Such anomalous behaviour serves to re-emphasize the importance of visually checking (using an oscilloscope) any signal for true Doppler modulation characteristics before relying on a frequency tracker output.

Since a complex scattering signal may contain frequency components within the passband of the tracker, an a priori knowledge that the signal is of Doppler origin is essential to ensure reliable results. Thus the tracking of a non-Doppler signal does not imply a malfunction of the tracker but rather a lack of the very expensive sophistication that would be required to determine the type of modulating waveform.

Under normal operating procedures the acquisition of a viable input is simple to check before automatic signal handling commences, any subsequent loss of Doppler modulation is usually readily apparent.

3.5.3 Flow Structure Determination with the Bubble Detector

Although unrelated to the present series of measurements, there is an additional use for the bubble detector which will be described. This application has not been explored experimentally, but may have some merit in the remote monitoring of flows.

Consider 3 pairs of capacitor plates AA', BB', CC', arranged around the circumference of a non-metallic tube carrying a flow with voids, depicted in Fig. 9. In this figure a single void is shown travelling along the axis of the tube and located as shown. Neglecting edge effects, only the capacitor formed by plates BB' will exhibit a change in capacity.

Forming the ratios $\frac{A+C}{B}$, $\frac{A}{B}$, and $\frac{C}{B}$ (where A, B and C refer to the instantaneous capacities between the plate pairs AA', BB' and CC', respectively), enables a correspondence table between these ratios, and a few types of flow to be drawn up, as shown in Fig. 10. In each case the capacity ratio is unique and may also have other distinguishable characteristics (such as a change in the actual capacities, for fixed ratios).

A set of capacitors as described here could be used for the remote sensing of flow characteristics by using 3 bubble detectors and making the appropriate arithmetic operations on their outputs as suggested by Fig. 10.

3.6 Processing the Doppler Signal

3.6.1 Frequency Determination

A brief description of the various methods that may be used to extract the Doppler frequency from the outputs of detectors 1 and 2 was given in Ref. 1. It was stated at that time that some form of automatic frequency determination was desirable from the points of view of both accuracy and efficiency. It is pertinent at this time to discuss the problems involved in processing a Doppler signal, together with the statistical limitations on accuracy and instrumental difficulties.

3.6.2 Typical Detector Signals and Their Frequency Components

Two typical detector output signals are shown in Figs. 11c and 11h; signal 11c being generated by particles 1 and 2 travelling along the X axis.

A view of the XZ-plane along the Y-axis (at Y=0), would show a beam overlap as indicated in Fig. 11a. The fringes will be of uniform contrast or visibility and the resulting detector's output will have a $1/e^2$ intensity envelope modulated at the Doppler frequency. Similarly particles 3 and 4 crossing the Y-axis obliquely would produce a signal waveform drawn in Fig. 11h.

It is important to note that maximum-modulation depth is produced only where the beams overlap with equal intensity. Thus conditions, as in 11f, result in a decrease in the number of useable fringes for data reduction.

Optical misalignment, unequal intensities and differing polarization planes for the two beams can also produce signals similar in nature to Fig. 11h.

The output signals shown in Figs. 11c and 11h are composites of the high and low frequency components shown in Figs. 11d and 11i, and 11e and 11j, respectively, the latter containing the velocity information. The signals shown in Fig. 11e consist of a single burst of frequency information for each scattering particle traversing the probe volume. These bursts will be randomly superposed being dependent on the arrival time of each scattering centre.

3.6.3 Accuracy Limitations

It can be shown (Ref. 3 and 4) that the accuracy to which the frequency may be obtained from any single signal burst is directly proportional to the number of useable cycles of Doppler information in the burst. This accuracy is independent of the processing technique employed.

The relative frequency/velocity error for n-bursts of Doppler modulated information containing on average N-cycles for processing will be

$$\frac{\Delta f}{f} = \frac{1}{N} \tag{8}$$

The error may of course be reduced in the normal statistical way by averaging over multiple signal bursts. Assuming the velocity is constant over an integration time of n signal bursts, we have for the average number $\bar{N}$ over the n-groups an error.

$$\frac{\overline{\Delta f}}{\bar{f}} = \frac{1}{\bar{N}\sqrt{n}} \tag{9}$$

It can be seen from this last equation that the accuracy scales more rapidly with N than n, hence the importance of arranging the optics for a maximum number of fringes.

3.6.4 The DISA Electronic Frequency Tracker

Canaden Products, Canadian representatives for DISA kindly provided a DISA electronic tracker for evaluation while the experiment was in progress.

The unit, described in Ref. 5, enables Doppler signals between 2 KHZ and 15 mHZ to be tracked continuously after pre-selection of the appropriate frequency range. The output voltage of the unit is linearly related to velocity and signal drop-out is displayed on a panel meter.

In principle the appropriate frequency range can be found employing a search technique using only the tracking unit, automatic tracking within certain limits is then provided after this has been accomplished. In actual operation using complicated signals (containing drop-outs etc.) an a priori knowledge of the approximate Doppler frequency is required to avoid spurious results.

On several occasions with detector signals composed of drop-outs and weak Doppler modulation the unit gave signal outputs even when the Doppler signal could no longer be observed on an oscilloscope. This anomalous

behaviour is not a fault of the system, but merely verification that when frequency components in any detector signals fall within the tracking bandpass, most frequency processors have insufficient discrimination to unequivocally determine if they are of Doppler origin.

Used with discretion, as any processor should be, the DISA frequency tracker is an excellent unit and will probably handle most of the preliminary requirements at AECL.

4. CONCLUSIONS

The experiments detailed in this report show the laser Doppler technique to be capable of providing accurate velocity measurements of both phases in a bubbly water flow even under quite turbid conditions.

The electronic instrumentation developed and constructed for this project provided automatic readout of the Doppler frequency and real-time void fraction measurements on the flow.

REFERENCES

1. Davies, W.E.R. — Velocity Measurements in Bubbly Two-Phase Flows Using Laser-Doppler Anemometry. UTIAS Technical Note No. 184, December 1972.

2. Foreman, J. W. — Optical Path Length Difference Effects in Photomixing with Multimode Gas Laser Radiation. Appl. Opt., Vol. 6, No. 5 (1967).

3. Greated, C. Durrani, T. S. — Signal Analysis for Laser Velocimeter Measurements. J. Phys. E. Sci. Instr., Vol. 4, p. 24 (1971).

4. Wilmshurst, T. H. — Resolution of the Laser Fluid Flow Velocimeter. J. Phys. E. Sci Instr., Vol. 4, p. 77 (1971).

5. Deighton, M. O. Sayle, E. A. — An Electronic Tracker for the Continuous Measurement of Doppler Frequency from a Laser Anemometer. DISA Information No. 12, Nov. 1971. Available from Canaden Products Ltd., Box 1411, Montreal 379, Tel. (514) 331-9360.

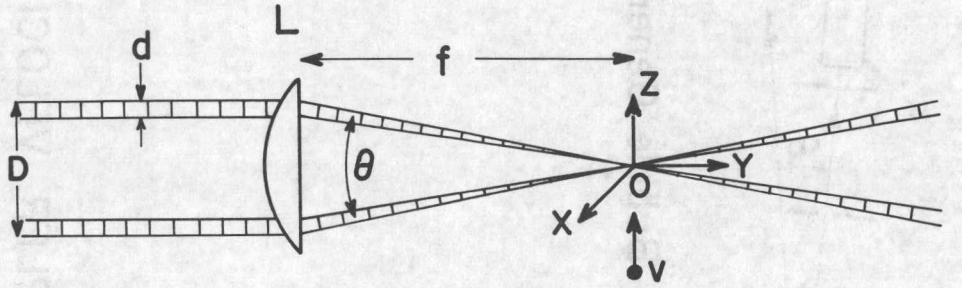

(a) Focussing Arrangement

Fringe Spacing

$$\delta = \frac{\lambda}{2 \sin \theta/2}$$

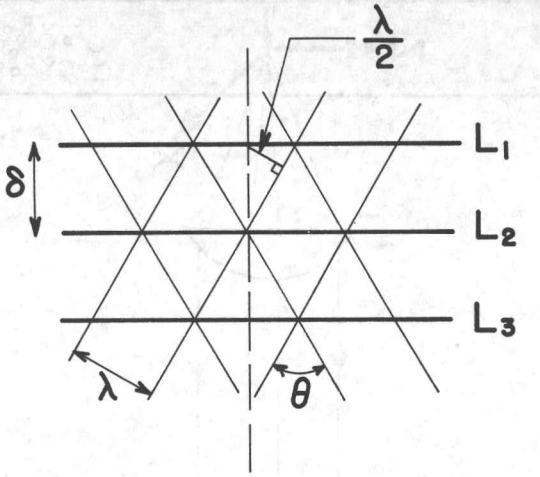

(b) Formation of Fringe Pattern

$\Delta X = d$

$\Delta Y = d/\sin\frac{\theta}{2}$

$\Delta Z = d/\cos\frac{\theta}{2}$

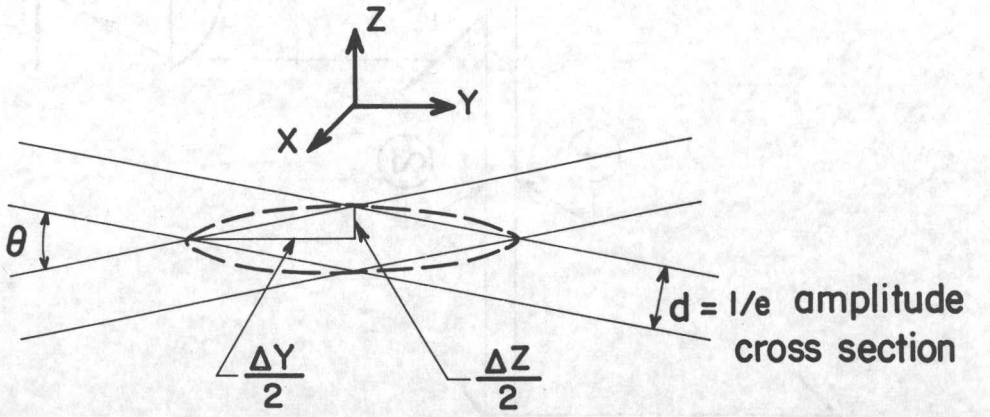

(c) Measurement Volume

FIG. 1 FOCUSSING GEOMETRY & FRINGE FORMATION

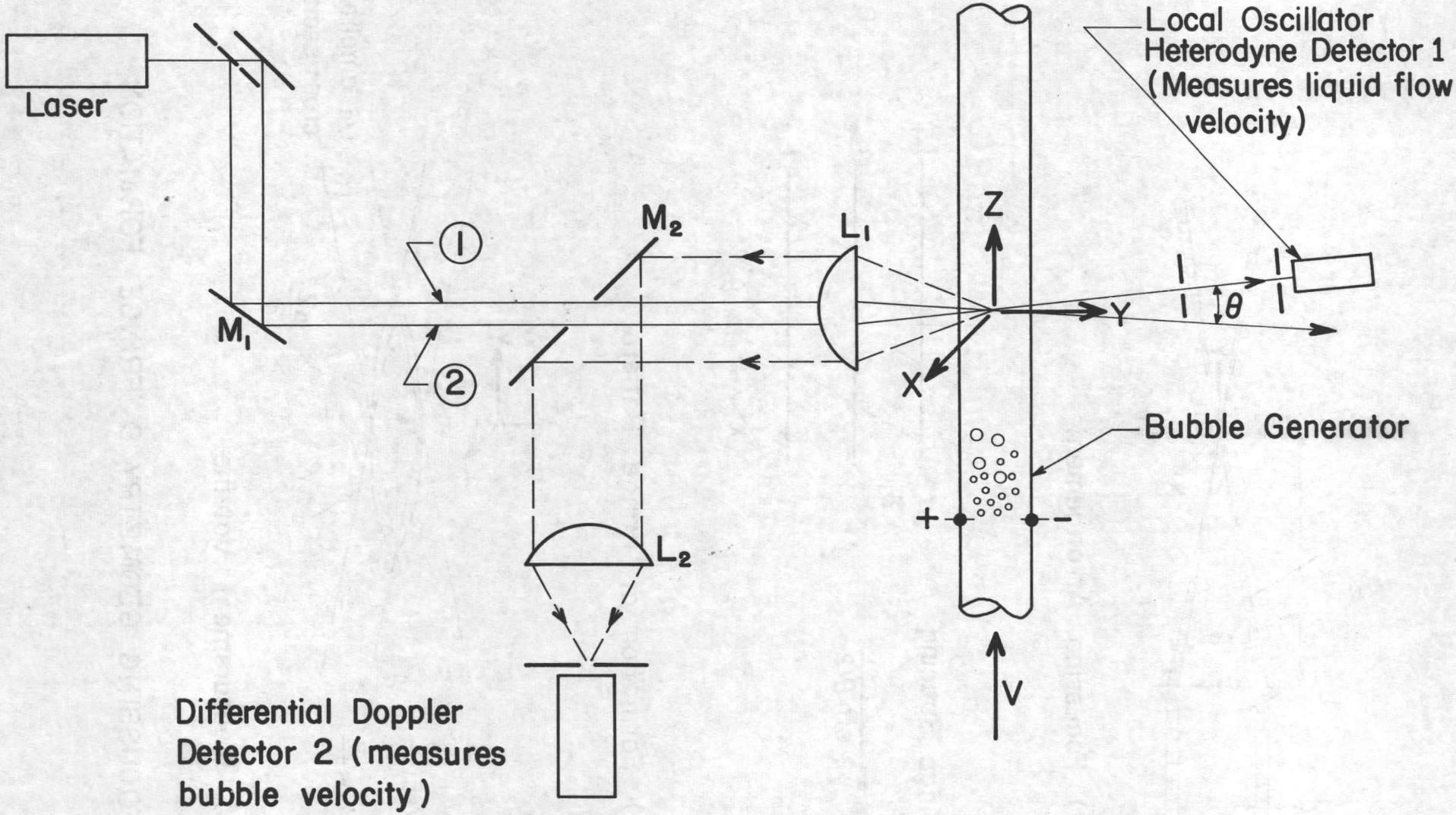

FIG. 2 EXPERIMENTAL ARRANGEMENT FOR MEASURING DOPPLER VELOCITIES OF WATER AND BUBBLES

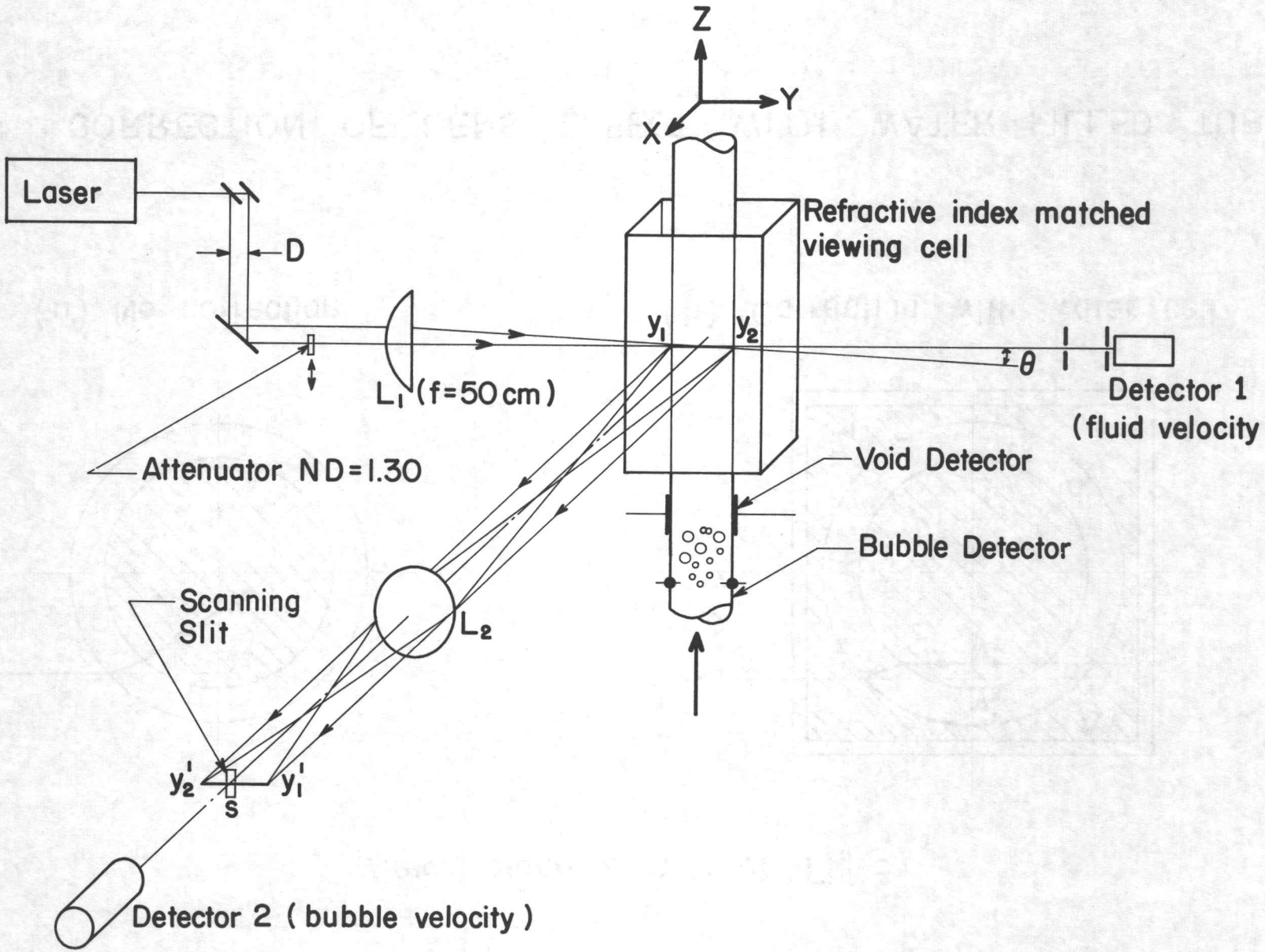

FIG. 3 EXPERIMENTAL ARRANGEMENT FOR VELOCITY DETERMINATIONS

Views along Z axis of Fig.3

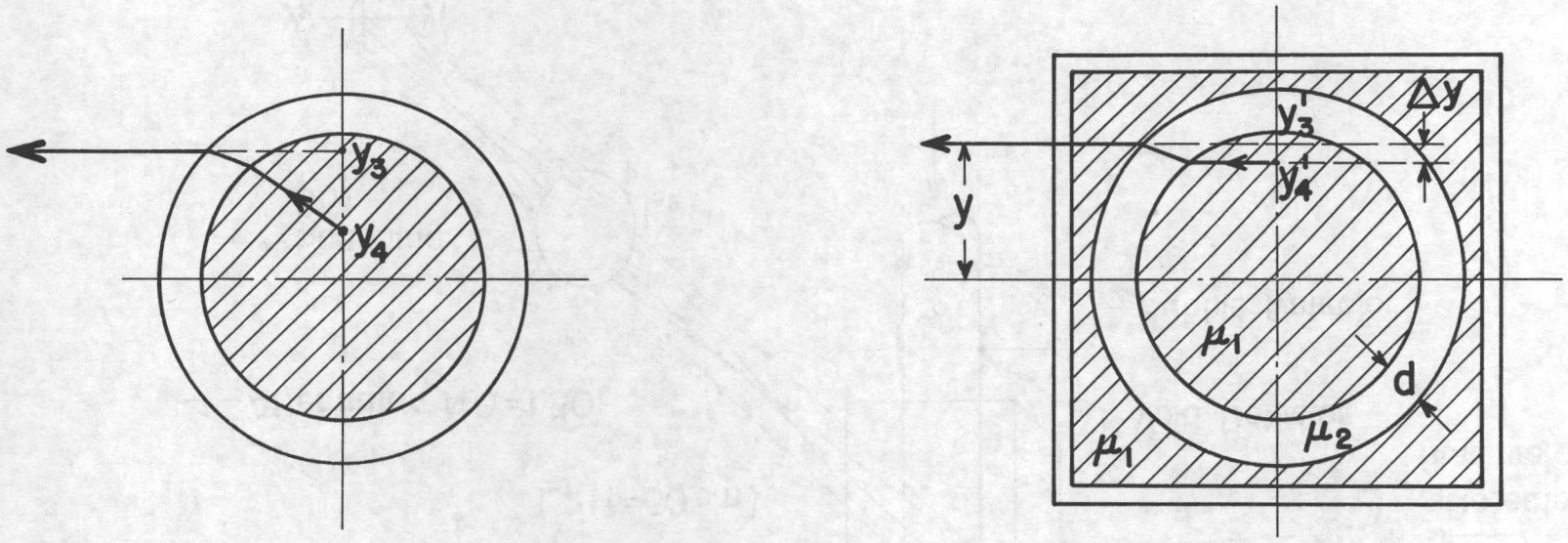

(a) No correction

(b) Correction with water cell

FIG. 4 CORRECTION OF LENS EFFECT WITH WATER FILLED TUBE

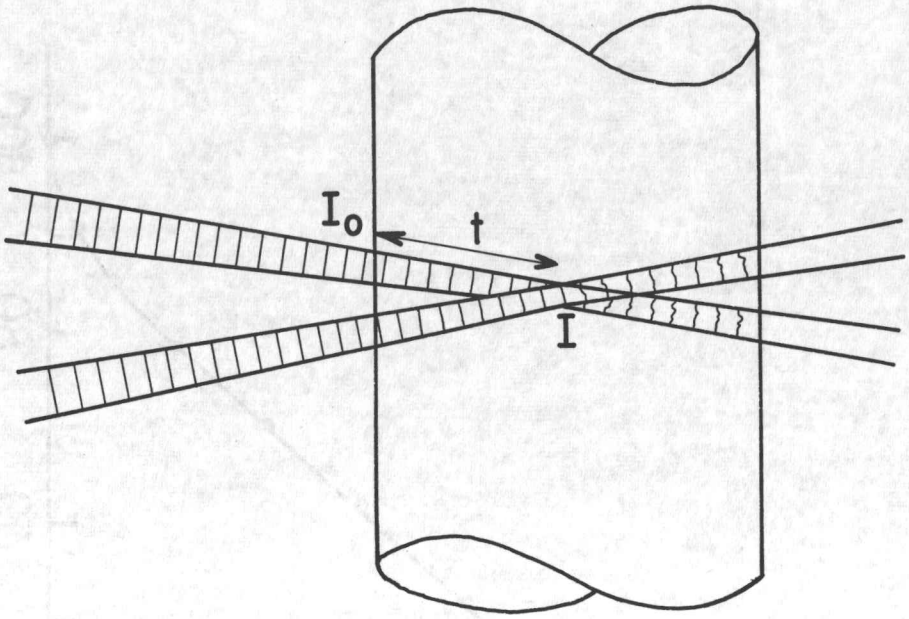

FIG. 5 DESTRUCTION OF COHERENCE DUE TO TURBIDITY

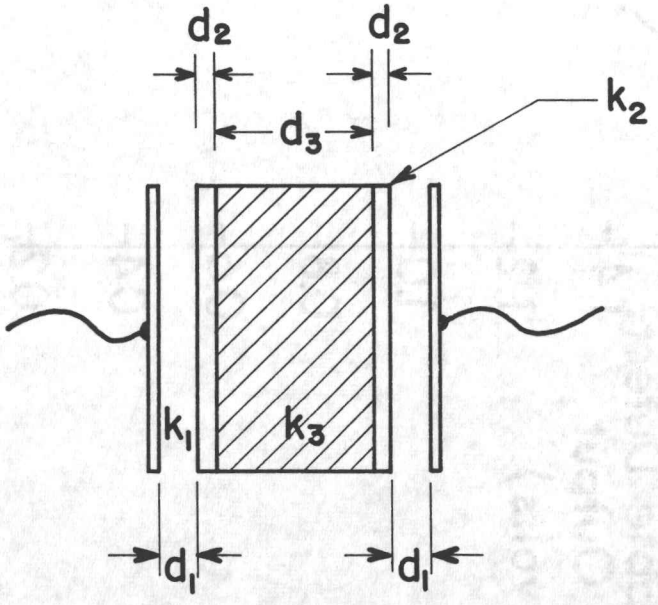

FIG. 6 BUBBLE DETECTOR DIMENSIONS

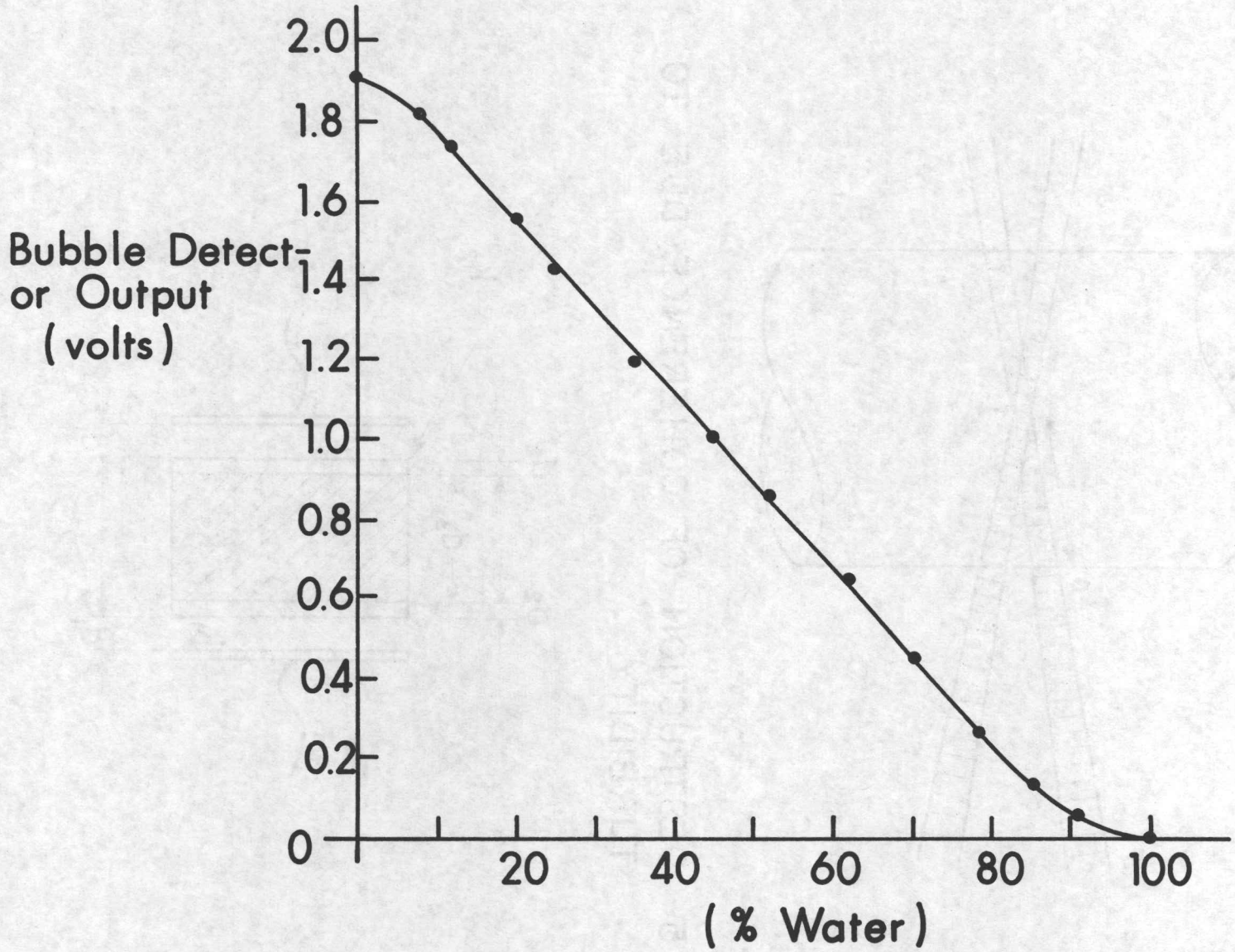

FIG. 7 BUBBLE DETECTOR CALIBRATION CURVE

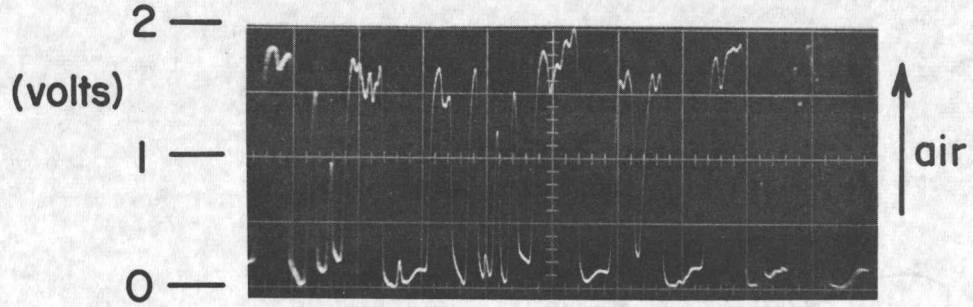

(.5 sec/cm)

(a) Big Bubbles (high pressure air input) Voids ~ 50%
liquid velocity = 30 cm/sec

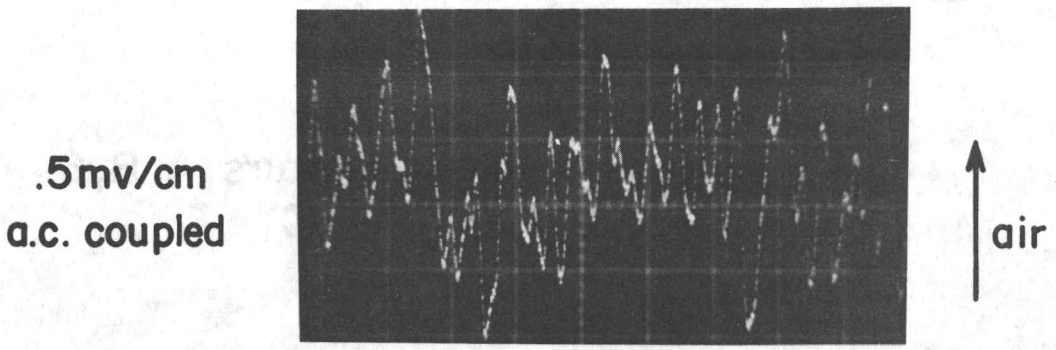

(.5 sec/cm)

(b) Small Bubbles (Electrolysis) Voids ~ 1%
liquid velocity = 22.5 cm/sec

FIG. 8 BUBBLE DETECTOR OUTPUTS

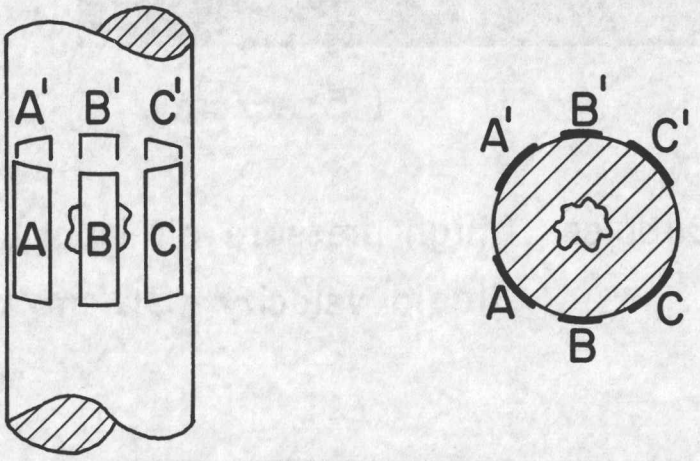

Capacity between plate pairs A, B, C
with no bubbles A = B = C

FIG. 9 CAPACITOR PLATE ARRANGEMENT FOR FLOW MONITORING

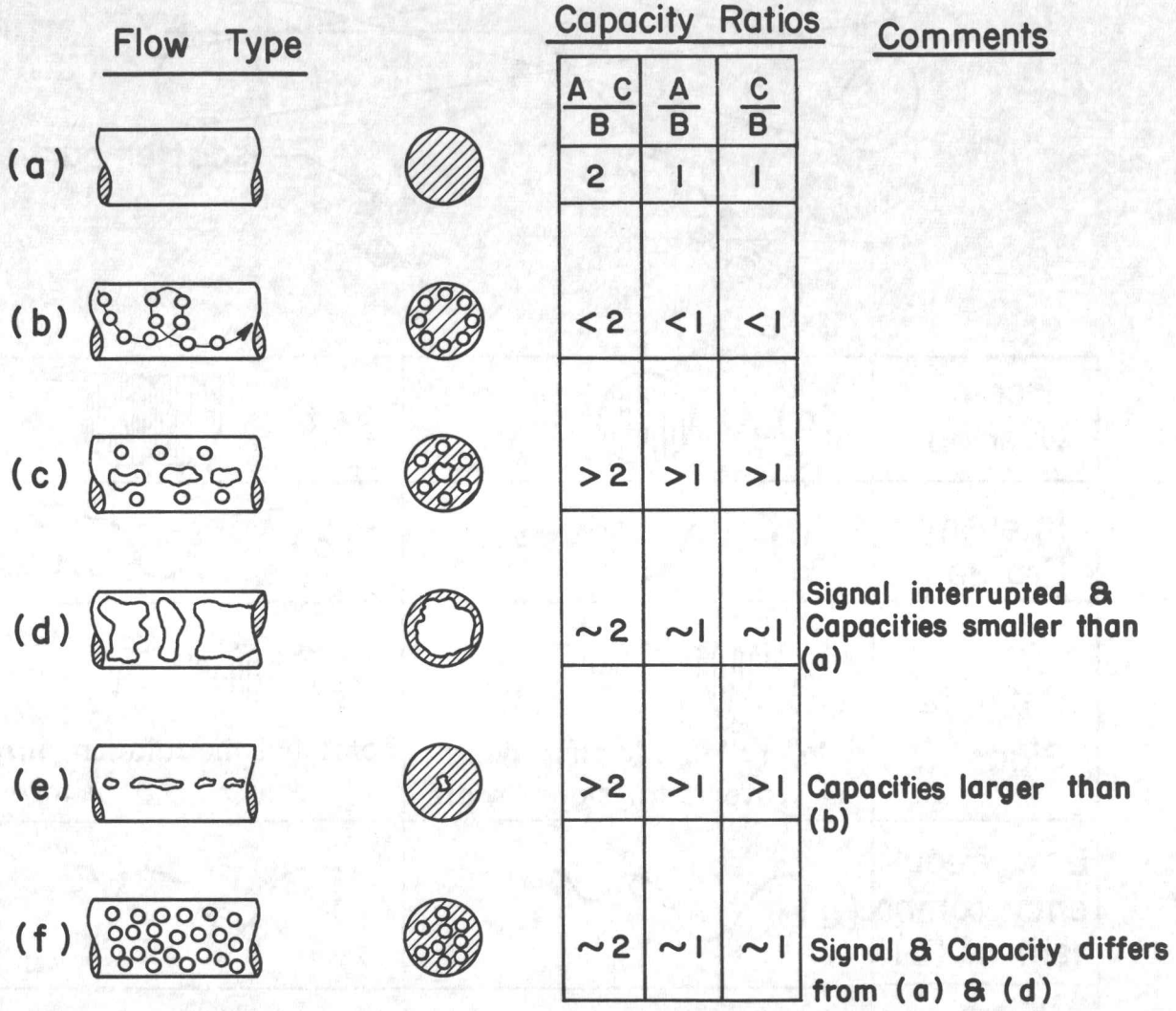

FIG. 10 DETERMINATION OF FLOW TYPE USING BUBBLE DETECTOR

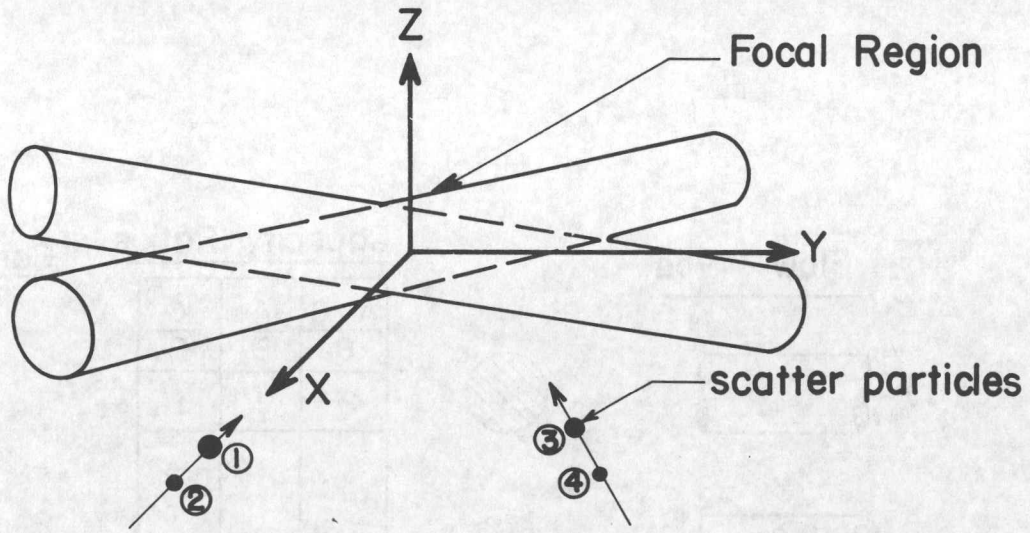

Beam Overlap	(a)	(f)
Intensity Profile	(b) $\frac{1}{e^2}$	(g) not $\frac{1}{e^2}$
Detector Signal	(c) note: full modulation depth over total signal width	(h) note: full modulation only over ~ 1/3 beamwidth
Low frequency component of (c)	(d)	(i)
High frequency component of (c)	(e) N=4	(j) trigger level N=2

FIG. II PRODUCTION OF TYPICAL DETECTOR SIGNALS & THEIR FREQUENCY COMPONENTS

APPENDIX A

DISCRIMINATOR FREQUENCY-TRACKER ELECTRONICS

A. INTRODUCTION

For quasi-continuous signals generated by flows with small velocity fluctuations, a simple frequency-to-voltage converter is one of the most economical methods of automatic frequency tracking. However, in general, flows are sufficiently complicated to require a more sophisticated approach.

The fastest tracker is that which can provide velocity information from the transit signal originating from a single particle. This approach requires handling single modulated intensity profiles and the discriminator system constructed at UTIAS is based on this principle. For situations where the velocity is changing very rapidly, as in some of the conditions anticipated at AECL, the discriminator method is probably the fastest, yielding automatically information otherwise obtainable only by the continuous monitoring of an oscilloscope.

The UTIAS discriminator-tracker covers the frequency range 5-100 KHZ without range switching, corresponding to flow velocities of 8-160 cm/sec for the experimental condition shown in Fig. 3. The tracker output was time-averaged for convenience during measurement, but it is capable of giving velocity information on a single particle traversing the probe volume.

B. DISCRIMINATOR FREQUENCY TRACKER, PRINCIPLE OF OPERATION

It has been shown in Section 3.6.3 that, within certain statistical limitations, the velocity of a scattering particle is defined by the Doppler frequency of a single signal-pulse burst. Figure Ala depicts a typical such pulse train after low-frequency components have been removed. At this stage it is merely necessary to measure the time periods τ_D between zero crossings to obtain the frequency.

In the discriminator approach, a pulse height level h, chosen to be above the A.C. noise, is selected as an arbitrary reference line. Crossings of this line by the signal waveform result in constant width and amplitude pulses (Fig. Alb), being formed by appropriate circuitry.

The Doppler frequency is then obtained by comparing the arrival rate of the pulses in Fig. Alb with those from a fixed clock (Fig. Alc), the latter's frequency being equal or higher than the maximum anticipated Doppler frequency.

For many purposes it is convenient to have an analog output which is proportional to the flow velocity. In this experiment this was arranged by integrating the pulse trains of Figs. Alb and Alc on capacitors C_1 and C_2 of the diagram. The ratio of the stored charges is then directly proportional to velocity and statistical accuracy may be varied by selection of C_1 and C_2.

Figure Al shows that the reference clock generator pulses start at the leading edge of the first signal pulse and end at the trailing edge of the last signal pulse. In practice this condition was difficult to achieve because of the problem of turning off the reference on the trailing edge of

the last pulse only. It was necessary to delay the reference pulses by 200 μsec as explained in the general description of operation.

C. GENERAL DESCRIPTION OF OPERATION

The signal at the P.M. (photo-multiplier) tube anode is amplified by the composite signal pre-amplifier (Fig. A2). This pre-amplifier also removes any D.C. background which may be superimposed on the P.M. signal.

The amplified output signal (Fig. A3a) is subsequently passed through a high-pass filter removing the laser intensity profile from the composite signal. The output of the high-pass filter is the Doppler-frequency component of the composite-input signal. This Doppler signal, now crossing zero, is amplified, then passed through a discriminator and pulse shaper to produce a series of output pulses of constant width and amplitude (Fig. A3 b, c and d).

A reference oscillator (Fig. A3ℓ) with an output frequency equal to the maximum trackable frequency (100 KHZ), and with its output shaped to produce pulses of the same width and amplitude as the signal pulses (Fig. A3d), is gated on for a time determined by the period of the signal pulses (Fig. A3m) available for measurement after the signal pulse train (Fig. A3d) has gone through the noise immunity circuit (shift register of Fig. A2).

The signal pulses (Fig. A3m) and the reference pulses (Fig. A3ℓ) are converted to analog-voltage levels by the signal D/A converter and the reference D/A converter (Fig. A2).

The two voltage levels from the D/A converters (Fig. A3 n and o) are compared by a log-ratio unit and the output voltage of the latter is proportional to the input Doppler frequency.

Noise immunity is provided by a shift register (Fig. A2), the output of which gates the signal pulse train to the signal D/A converter only at the leading edge of the third consecutive pulse coming in at rate of 5 KHZ or greater (Fig. A3 d and m).

The reference oscillator turn on, scheduled to start at the leading edge of the first pulse of Fig. A3m, is delayed for 200 μsec (Fig. A3 m and ℓ). This is necessary because the reference oscillator is turned off when the shift register (Fig. A2) is reset 200 μsec after the last pulse of the signal pulse train (Fig. A3 d, e, f and ℓ). This time corresponds to an absence of a signal pulse at the lowest Doppler frequency intended for measurement (5 KHZ).

A signal averaging timer allows an average frequency measurement over a variable period of time to be made. This timer controls the reset of the D/A converters and is triggered from the shift register output.

D. DETAILED DESCRIPTION OF OPERATION

1. Composite-Signal Pre-Amplifier

The composite signal pre-amplifier consists of a voltage follower (Fig. A4 Q1) and a high gain (40 DB) broad-band amplifier (Fig. A4 Q2). The voltage follower Q1 is A.C. coupled to Q2 to remove any D.C. background which may be on the P.M. tube signal. The composite signal pre-amp output voltage should be between 1 and 10 volts peak (Fig. A3a) for proper circuit operation.

The output of amplifier Q2 is available for monitoring purposes (MON 1) with an oscilloscope. The input signal should be adjusted for operation between 1 and 10 volts peak.

The two resistors marked RT (Fig. A4 Q2) are intended for amplifier offset adjustment. (Refer to amplifier specification for proper procedure.)

2. High-Pass Filter

The composite signal at the pre-amplifier output consists of two components: the Doppler frequency and the intensity profile (Fig. A3a). The high-pass filter removes the intensity profile and leaves the Doppler frequency for analysis. This filter action takes place because for any composite signal, the intensity profile, having lower frequency components than the Doppler frequency, is attenuated more than the Doppler frequency.

The high-pass filter is comprised of a 5 pF capacitor and a 1 kΩ resistor (Fig. A4) to produce a very short time constant (5 nano seconds) with respect to the time period of the Doppler frequencies intended for measurement (5 KHZ = 200 μ/S, 100 KHZ = 10 μ/S). Assuming a pre-amplifier output of 10 volts peak, the high pass filter output at 5 KHZ would be 1.5 millivolts peak to peak and at 100 KHZ the output would be 30 millivolts peak to peak.

3. Doppler-Signal Amplifier

The Doppler-signal amplifier consists of discrete component amplifier Q3, Q4, Q5, Q6, Q43 and amplifier Q7 (Fig. A4). The gain of the discrete amplifier is in excess of 70 db at 100 KHZ. The high-pass filter output at 100 KHZ is 30 mv peak to peak (Q2 output = 10V) resulting in saturation of the discrete amplifier. Operation in this mode is desired because if the input composite signal at the P.M. tube anode dropped by a factor of 10, the discrete amplifier output would still be in excess of 9 volts.

At 5 KHZ, the high-pass filter output is only 1.5 millivolts peak to peak (Q2 output 10V). The discrete component amplifier gain at 5 KHZ is 75 db, resulting in an output of 8 volts peak to peak. However, as in the 100 KHZ example, if the composite signal at the tube anode dropped by a factor of 10, the output of the discrete amplifier would be 800 millivolts peak to peak. This is insufficient amplitude to trigger the discriminator. Amplifier Q7 (Fig. A4) overcomes this difficulty by providing an additional gain of 11 to the signal. The 800 millivolts is thus presented as 8.8 volts peak to peak at Q7 output. Diodes D3 and D4 prevent Q7 from saturating while the .0075 μF capacitor across the diodes provides a low impedance path to ground for high frequency noise.

In general, when measuring Doppler frequencies in excess of 20 KHZ, the discrete amplifier output should be used to feed the discriminator while for frequencies between 5 and 20 KHZ the output of Q7 (Fig. A4) should be used. This selection is accomplished by switch S1 (Fig. A4). The amplifier output is illustrated in Fig. A3b.

4. Discriminator

The discriminator is composed of Q8, Q9, Q10 and associated circuitry (Fig. A4). This circuit is a Schmitt trigger (Q8, Q9) with an emitter follower output stage (Q10). The circuit has a basic trigger level of 1 volt with additional adjustment provided by the 100 kΩ input potentiometer.

Diode D5 (Fig. A4) limits the negative signal excursion on the base emitter junction of Q8 to prevent destruction under large signal conditions.

Emitter follower Q10 provides a low output impedance for the detected pulses (Fig. A3c). The trigger level should be adjusted to be above the level of the peak noise.

5. Pulse Shaper

The pulse shaper is a push-pull multi-vibrator composed of transistors Q11, Q12, Q13, Q14 and associated components (Fig. A4). Push-pull operation is desirable because it reduces the effects of transistor-storage capacity and provides a very low output impedance.

The output amplitude and pulse width are 10 volts and 4 μ/S respectively (Fig. A3d). The pulse shaper produces one output pulse for each negative going transition on Q11 base. Decoupling from the 10 volt supply is provided by a 10 Ω resistor and 100 μF capacitor (Fig. A4).

The output of the pulse shaper, available for monitoring purposes (MON 2) with an oscilloscope, should be observed while adjusting the trigger level of the discriminator.

6. Signal D/A Converter

The signal D/A converter changes the Doppler signal pulse train (Fig. A3d) into an analog voltage level. The circuit consists of transistors Q15, Q16, Q34, mos-fet Q17, amplifier Q18 and associated components (Fig. A4). The 10 volt 4 μsec Doppler signal pulses charge capacitor C_s through constant current source Q16. The charging current is regulated at 7.5 μa per signal pulse to produce a voltage across capacitor C_s of approximately 64 μV per signal pulse.

Amplifier Q18 operates at a gain of 2.5 and isolates the voltage charge on capacitor C_s from the log ratio unit input impedance.

Diode D6 (Fig. A4) prevents the voltage charge on capacitor C_s from leaking to ground through the collector base junction of Q16.

As discussed in General Description of Operation, noise immunity is achieved by keeping the D/A converter gated off until the third consecutive signal pulse arrives at a rate of at least 5 KHZ. Transistor Q15 performs this gating function by shorting out the D/A converter input until the leading edge of the third signal pulse from the pulse shaper (Fig. A3 d and m). At this time Q15 becomes an open circuit because its base signal from the shift register (Fig. A4 Q26) drops to zero volts (Fig.A3i).

Initially, mosfet Q17 is in a shorted condition. The signal averaging timer (Fig. A4 Q27) controls the state of Q17 (shorted or open). This timer, triggered at the leading edge of the third signal pulse (Fig. A3 d and k), turns on transistor Q34 reducing Q17 gate source voltage to 200 millivolts. This causes Q17 to turn off, allowing capacitor C_s to charge. Q17 remains off for a period of time determined by the signal averaging timer. The D/A converter input signal pulses and output voltage are illustrated in Fig. A3 m and n.

7. Reference Oscillator

The reference oscillator is a quad two input nor gate connected as a free-running multi-vibrator. Transistors Q38, Q39, Q40 and associated circuitry constitute a push-pull output switch. The oscillator frequency and pulse width are adjusted to 100 KHZ and 4 µsec respectively by varying the 620 pF feedback capacitors associated with gates 1 and 2 (Fig. A4 Q41). The oscillator drives the push-pull output switch to produce 10 volt 4 µsec reference pulses.

As explained in general description of operation, the reference pulses entering the reference oscillator D/A converter (Fig. A3ℓ) are delayed by 200 µsec from the first signal pulse entering the signal D/A converter (Fig. A3 m and ℓ). Transistor Q29, in association with the reference delay timer (Fig. A4 Q28) inhibits the oscillator for the additional 200 µsec while Q42 turns off the reference oscillator 200 µsec after the last signal pulse (Fig. A3d).

The reference output pulses are available for monitoring purposes with an oscilloscope (MON 3).

8. Reference Oscillator D/A Converter

The reference oscillator D/A converter composed of Q37, Q35, Q36, Q44 and associated components (Fig. A4) changes the reference pulse train (Fig. A3ℓ) into an analog voltage (Fig. A3o). Operation is identical to that of the signal D/A converter discussed previously.

Mosfet Q35 is opened at the same time as Q17 of the signal D/A converter by the signal averaging timer, allowing capacitor CR to be charged by the reference pulses (Fig. A3ℓ).

9. Shift Register Reset Timer

The shift register reset timer, composed of Q19, to Q24, diodes D15, D16 and associated components (Fig. A4) controls the output state of shift register Q26 (Fig. A4), which in turn controls the time that the signal D/A converter is gated on (Fig. A3m) and the time period of reference pulses (Fig. A3ℓ).

Under no signal conditions, the 0.015 µF capacitor from Q21 non-inverting input to ground (Cx) is charged to 10 volts which turns Q24 on thus grounding the shift register reset line (Fig. A3f). The first signal pulse at the pulse shaper output (Fig. A3d) turns on switches Q19 and Q20 shorting capacitor Cx which causes Q21 output to fall below the trigger level of tunnel diode D16 (Fig. A3e). Subsequently Q24 turns off allowing signal pulses (Fig. A3d) to clock Q26 (Fig. A3f).

Repetitive signal pulses (Fig. A3d) occurring at a minimum rate of 5 KHZ limit the charge on CX below the trigger level of D16, allowing Q26 (Fig. A4) to remain in its clocked state. When the signal pulse arrival rate decreases below 5 KHZ, the lowest Doppler frequency intended for measurement, capacitor CX charges to the trigger level of D16 causing Q24 to turn on (Fig. A3 e and f) resetting shift register Q26 (Fig. A3 h and i).

10. Shift Register

The shift register, composed of Q25, Q26 and associated components (Fig. A4) provides timing for the signal averaging timer and the 200 µsec) reference delay timer, controls the gating of the signal pulse train to the signal D/A converter (Fig. A3 d and m) and controls the turn off of reference oscillator Q41.

The signal pulse train (Fig. A3d) provides positive transition clocking through Q25. The first pulse of Fig. A3d does not alter the state of Q26 because the reset line is grounded for the entire positive going leading edge (Fig. A3 d, e and f).

During the leading edge of the third signal pulse (Fig. A3d), the shift register outputs change state (Fig. A3 h and i) causing the signal D/A converter gate switch Q15 to open, allowing signal pulses starting with the third pulse (Fig. A3 d and m) to be converted to analog information. The reference oscillator inhibit transistor Q42 is also opened but the reference oscillator is inhibited for an additional 200 µsec by the reference delay timer (Q28 Fig. A4), which receives a trigger pulse from the shift register output (Fig. A3h).

The shift register output (Fig. A3h) also triggers the signal averaging timer which opens the signal and reference D/A converter reset switches (Q17, Q35 Fig. A4) allowing signal processing.

Resetting of the shift register takes place in the absence of a signal pulse in 200 µsec (corresponding to the time period of the lowest frequency of measurement 5 KHZ) when Q24 of the reset timer turns on shorting out the reset line of Q26.

11. Reference Delay Timer

The purpose of the reference delay timer (Q28, Q29 and associated components, Fig. A4) is to eliminate the 200 µsec time period of excess reference pulses which would be present in the absence of this circuit. This excess of reference pulses is produced because the shift register Q26 and consequently the reference oscillator is not inhibited for a period of 200 µsec from the last signal pulse (Fig. A3 d and f).

By inhibiting the reference for an additional 200 µsec from the leading edge of the third pulse of waveform A3d, the error is eliminated. The net result is that the reference oscillator pulses are shifted in time from the signal pulse (Fig. A3 ℓ and m).

The reference delay timer receives its trigger pulse from the shift register output (Fig. A3h). Transistor Q29 inhibits the reference oscillator for the additional time period of 200 µsec (Fig. A3j).

12. Signal Averaging Timer

The signal averaging timer is composed of Q27, Q30, Q31, Q32, Q33 and associated components (Fig. A4). This timer opens the D/A converter reset switches (Q17, Q35 Fig. A4) to allow the signal and reference pulse trains to be converted to analog information. This ON time, or measurement time is controlled by monostable multi-vibrator Q27, which receives its trigger pulse from the positive transition of the shift register (Q26) output (Fig. A3h).

Provision is also made for a variable OFF time or non-measurement time, when the timer output (Fig. A3k) is at zero volts, resulting in the D/A converter reset switches remaining in the on or shorted state. This time is determined by Q32 (Fig. A4) which shorts out any trigger pulses to Q30 for a period of time determined by the CR time constant in the gate circuit of Q32. This CR network receives its voltage charge turning Q32 on from the previous on cycle of the multi-vibrator Q27.

The on and off times are individually adjustable to meet the requirements of the user.

13. Log Ratio Unit

The log ratio unit (Fig. A5) is a standard two operational amplifier circuit employing transistors connected in the trans-diode configuration. For detailed description refer to Analog Devices application note entitled "Design of Temperature Compensated Log Circuits Employing Transistors and Operational Amplifiers".

Operational amplifier Q1 receives its input from the signal D/A converter (Fig. A4) while Q2 receives its input from the reference D/A converter (Fig. A3 n and o).

The output of the log ratio unit is illustrated by the calibration curve of Fig. A7, where output voltage is plotted versus frequency and velocity.

14. Power Supply

The frequency tracker requires three regulated power sources: +15 VDC, -15 VDC and +10 VDC. Figure A6 illustrates the power supply schematic, where the two 15 volt regulated supplies are produced by Q1, and the 10 volt supply is produced by Q2, Q3 and associated components.

The unregulated DC input voltages must not exceed 40 VDC peak or drop below 20 VDC minimum.

E. OPERATION AND CALIBRATION

A signal generator duplicating the Doppler modulated intensity profile was designed and built to calibrate the instrument. The intensity profile repetition rate and width, the Doppler frequency and the output amplitude were all independently variable.

Figure A7 illustrates the calibration curve for the frequency tracker. With the Doppler input frequency held constant, intensity profile rate and width as well as input signal amplitude were varied independently and simultaneously. The output voltage remained constant during these tests (± 3%).

However, it was noted that when the profile repetition rate exceeded 5 KHZ, large errors were registered at the output. This is due to the fact that shift register reset timer Q21 (Fig. A4) does not reset under this condition (Fig. A3e), which allows the reference oscillator to run continuously. The instrument is therefore limited to measuring intensity profiles containing Doppler frequencies at profile repetition rates of 5 KHZ or less.

FREQUENCY TRACKER SEMICONDUCTOR PARTS LIST

Q1	QFT-2	Philbrick Nexus
Q2	Q82AH	Philbrick Nexus
Q3, Q4	2N2920	Motorola
Q5	MPS6519	Motorola
Q8, Q43	MPS6515	Motorola
Q6	MPS6518	Motorola
Q7, Q27, Q28	MC1433G	Motorola
Q9, Q10, Q15	MPS2369	Motorola
Q22, Q23, Q24	MPS2369	Motorola
Q25, Q29, Q31	MPS2369	Motorola
Q40, Q42	MPS2369	Motorola
Q11, Q12, Q16, Q37	MPS3640	Motorola
Q13, Q30, Q38	2N4403	Motorola
Q14, Q19, Q20	2N4401	Motorola
Q33, Q34, Q36, Q39	2N4401	Motorola
Q17, Q35	3N171	Motorola
Q18, Q44	1023/01	Philbrick Nexus
Q21	MC1741CG	Motorola
Q26	SP321A]	Signetics
Q32	M-103	Siliconix
Q41	SP380A	Signetics
D1 to D14	IN4148	Motorola
D15	IN270	
D16	IN3715	

LOG RATIO UNIT SEMICONDUCTOR PARTS LIST

Q1, Q2	1023/01	Philbrick Nexus
Q3	4357	Philbrick Nexus

REGULATOR SEMICONDUCTOR PARTS LIST

Q1	2101	Philbrick Nexus
Q2	MJE521	Motorola
Q3	MFC6030	Motorola

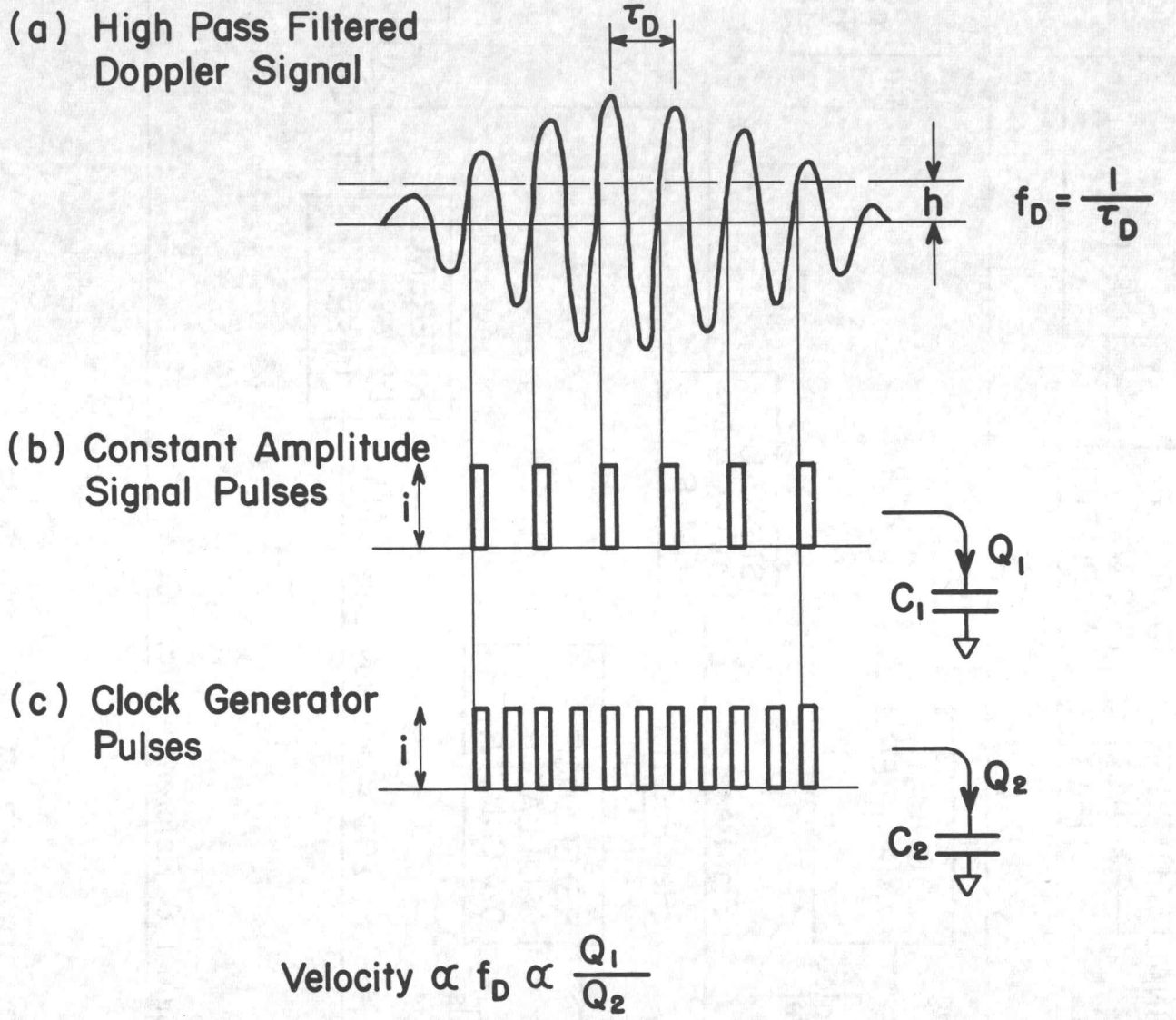

FIG. A1 DISCRIMINATOR FREQUENCY TRACKER OPERATING PRINCIPLE

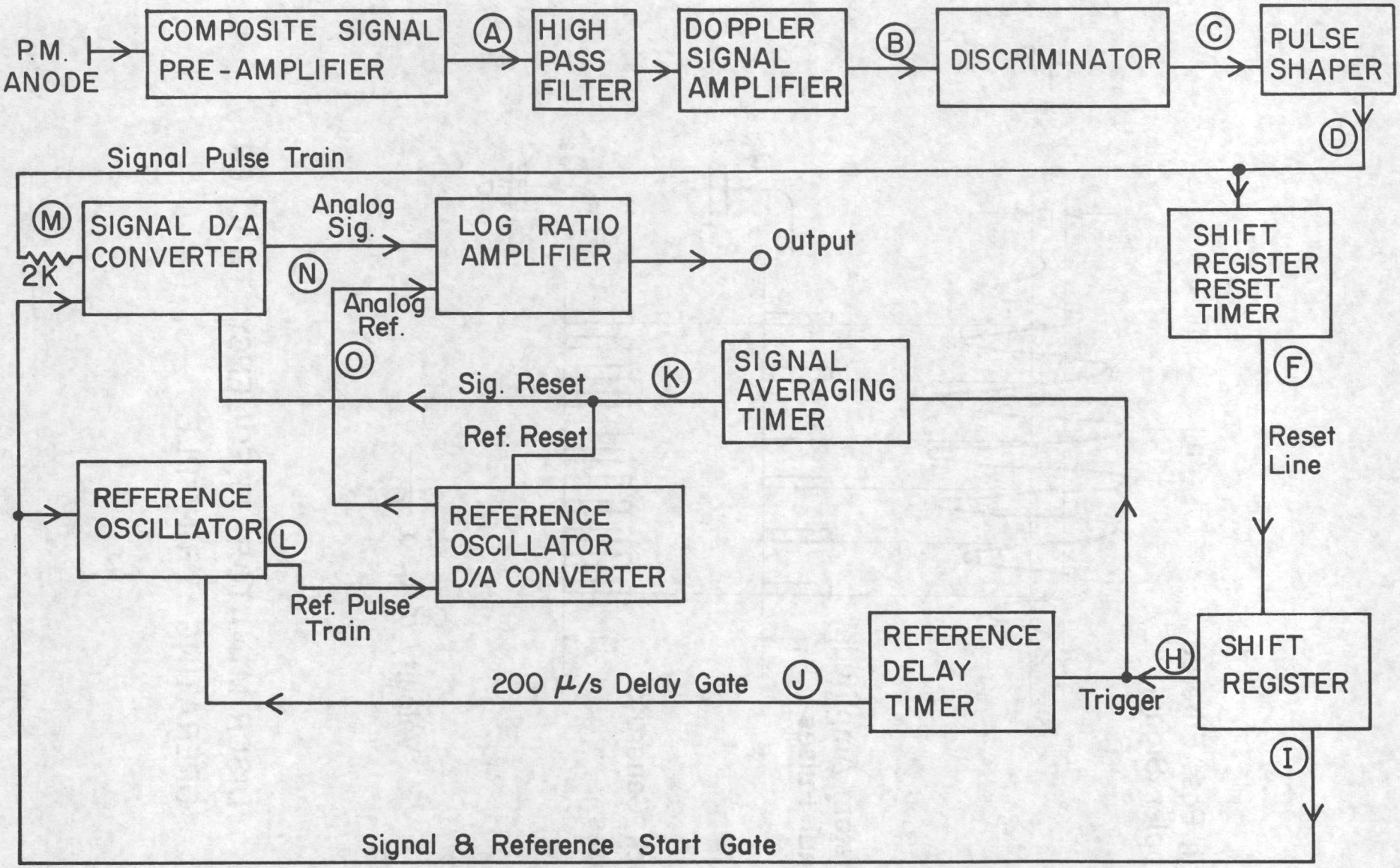

FIG. A2 FREQUENCY TRACKER BLOCK DIAGRAM

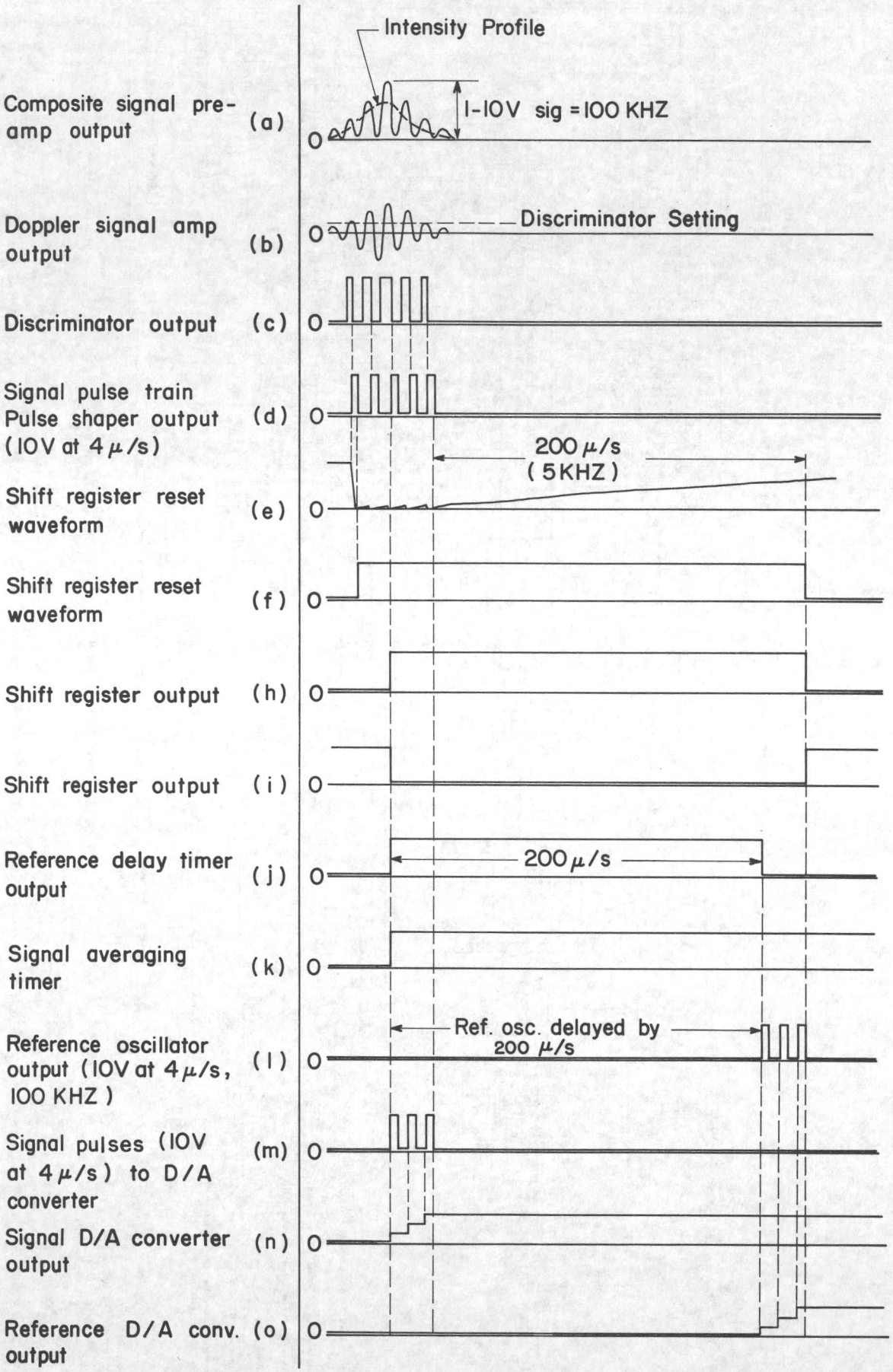

FIG. A3 FREQUENCY TRACKER WAVE FORMS

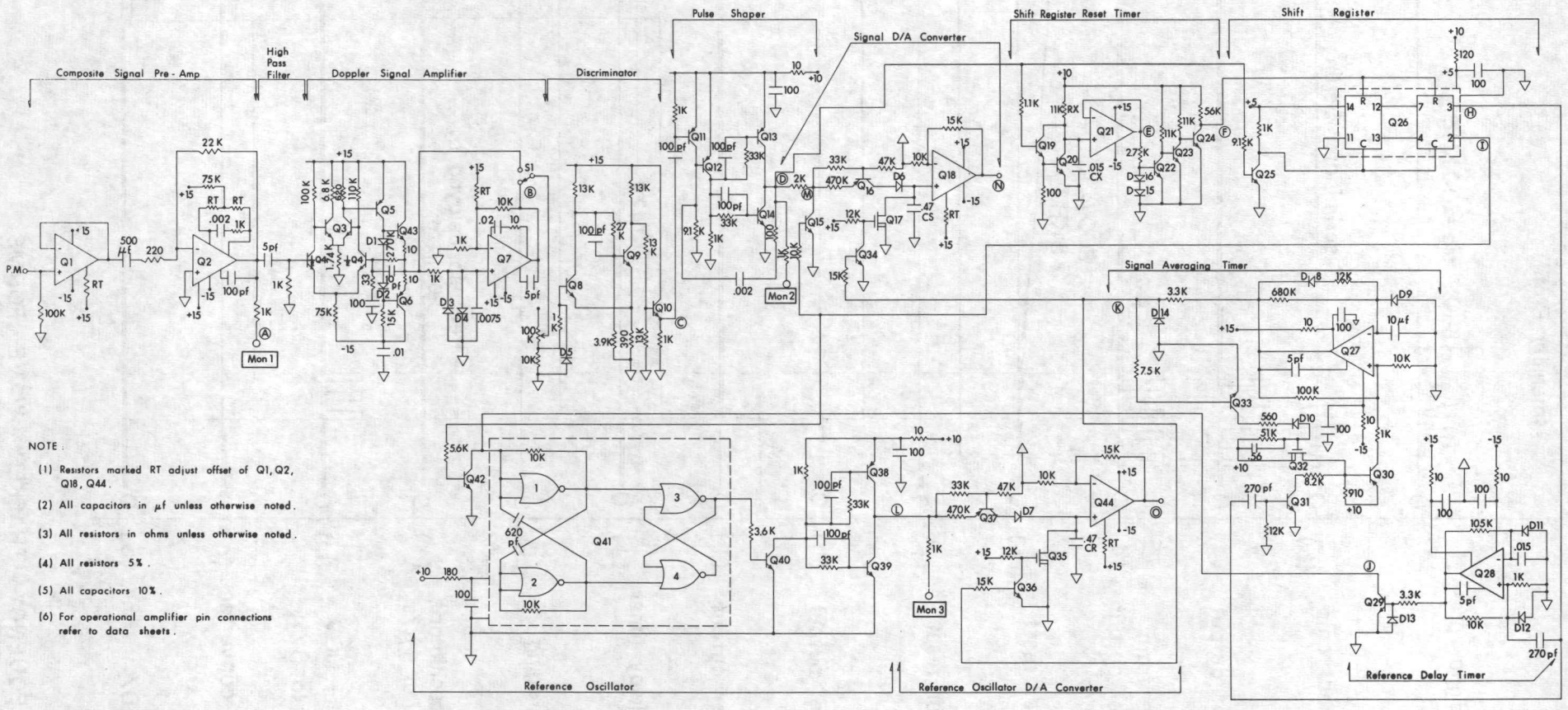

NOTE :

(1) Resistors marked RT adjust offset of Q1, Q2, Q18, Q44.

(2) All capacitors in μf unless otherwise noted.

(3) All resistors in ohms unless otherwise noted.

(4) All resistors 5%.

(5) All capacitors 10%.

(6) For operational amplifier pin connections refer to data sheets.

FIG. A4 FREQUENCY TRACKER SCHEMATIC

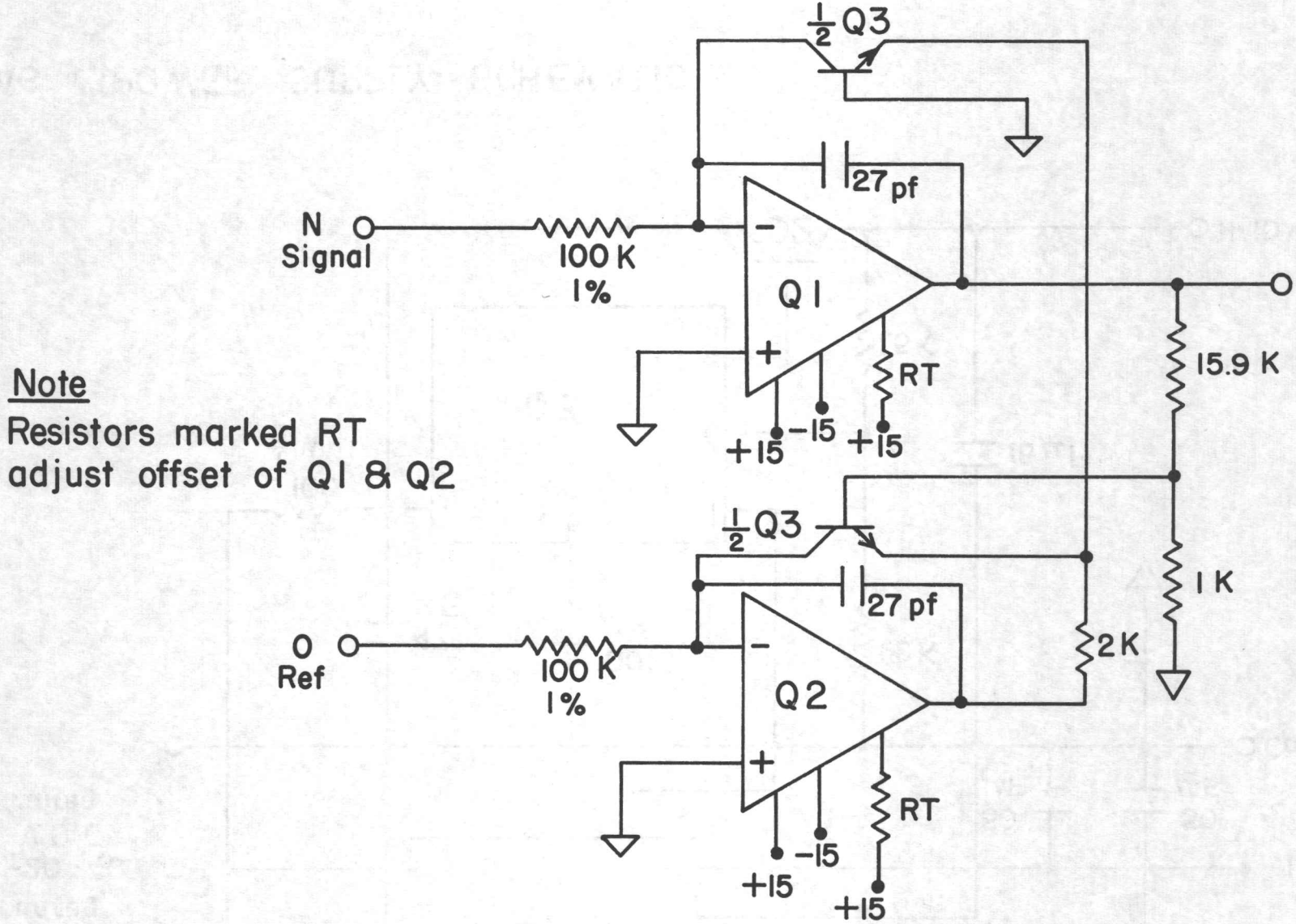

Note
Resistors marked RT
adjust offset of Q1 & Q2

FIG. A5 LOG RATIO UNIT SCHEMATIC

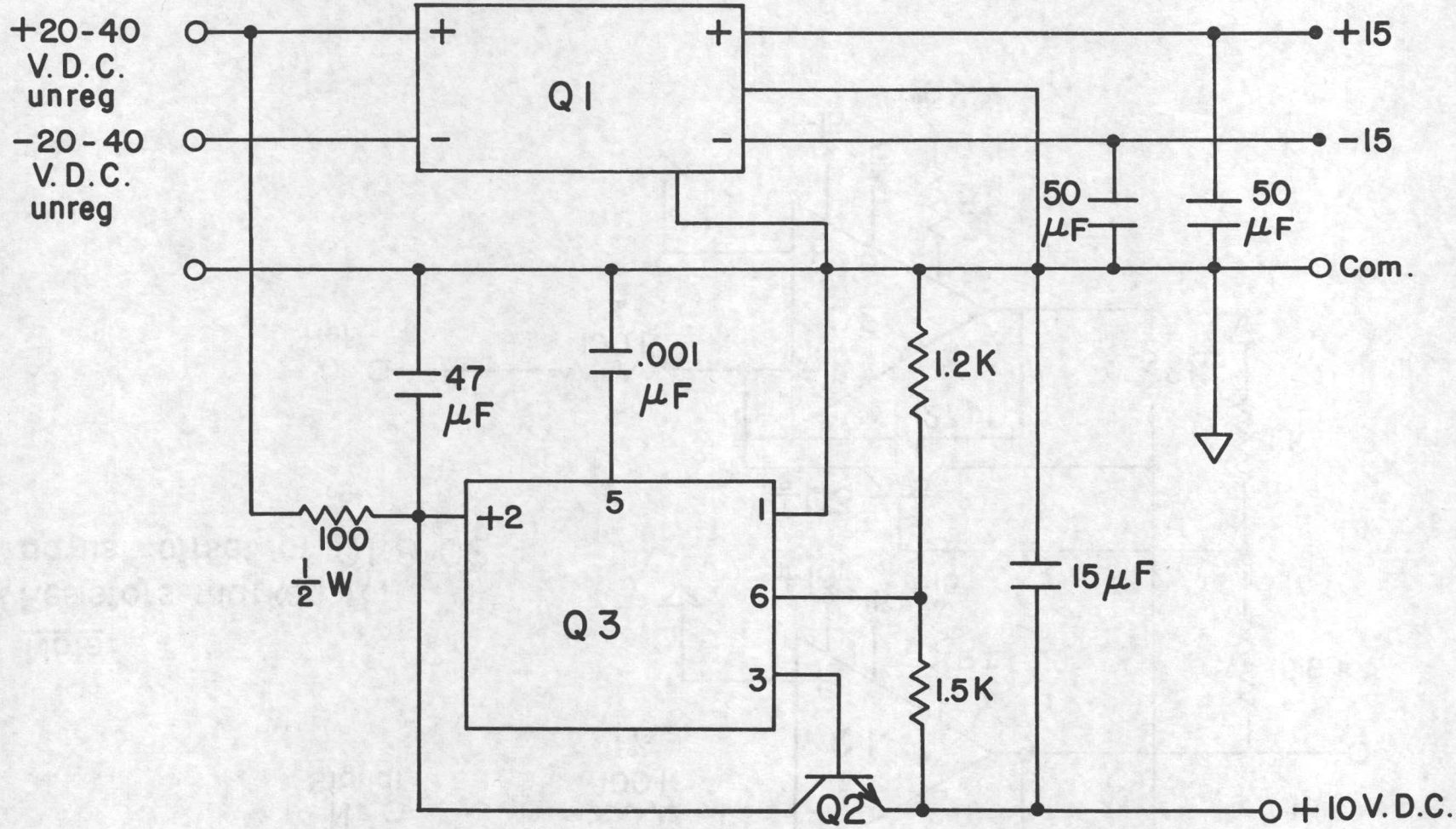

FIG. A6 POWER SUPPLY SCHEMATIC

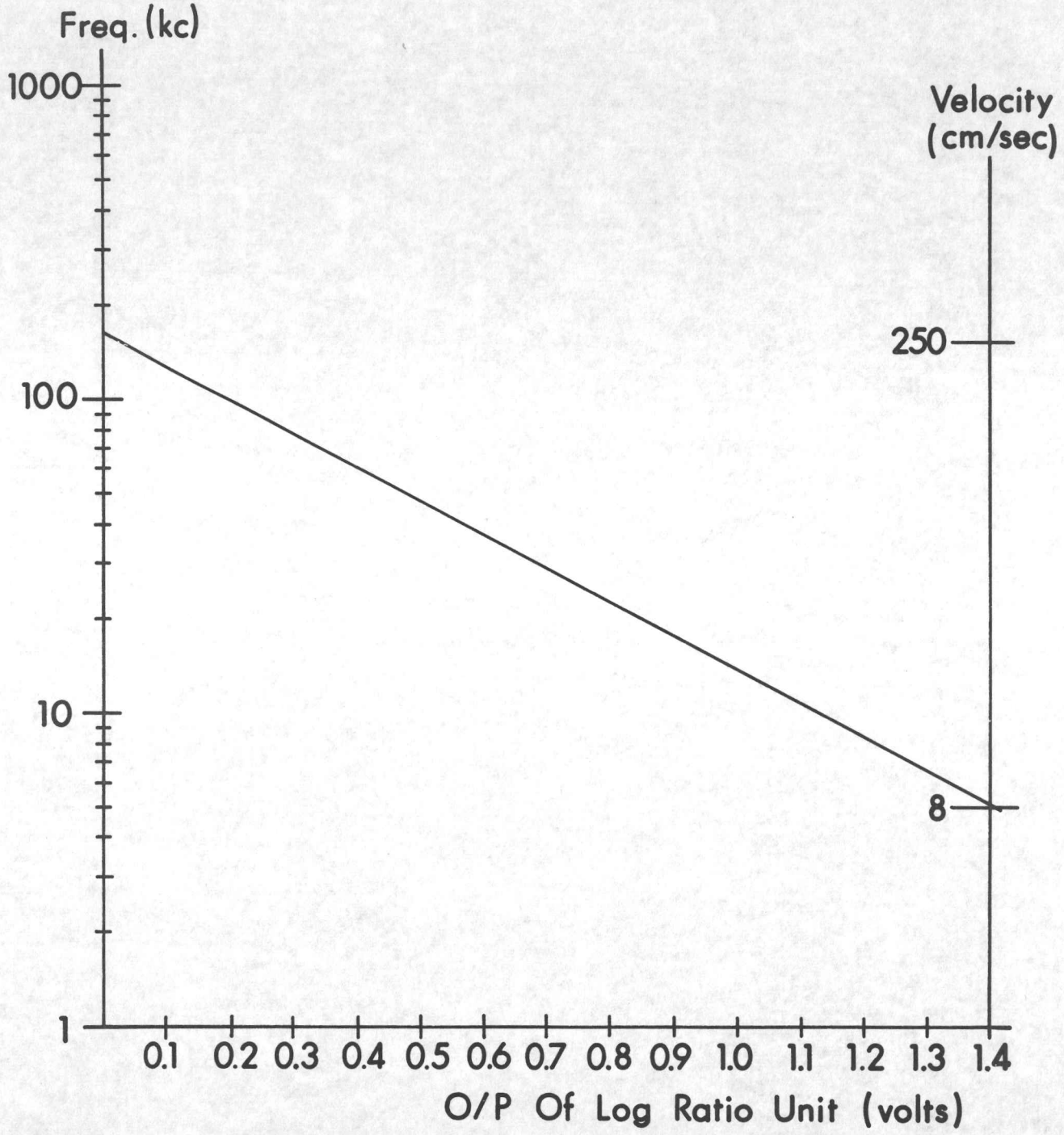

FIG. A7 LOG RATIO CALIBRATION CURVE

APPENDIX B

BUBBLE-DETECTOR ELECTRONICS

A. INTRODUCTION

The operating principle of the bubble detector has been discussed earlier in this report. The electronics measures a small capacity change with high-frequency response.

Commercial instrumentation for capacity measurement was investigated and found to be lacking in frequency response. This applied to such devices as capacitance bridges and Q meters, where the measurement response time was in excess of 100 msec. For this reason, instrumentation referred to as bubble detector electronics was developed with the required frequency response (10 KHZ).

B. PRINCIPLE OF OPERATION

The bubble-detector electronics is essentially a capacitance-to-voltage converter. The desired information contained in the capacity change of C1 (Fig. B1) is converted to an FM modulation of a HF (high frequency) oscillator (Fig. B1a). The FM modulated oscillator signal is demodulated by a quadrature detector (Fig. B1b) to produce an output signal directly proportional to the change in capacity of C1.

C. DETAILED DESCRIPTION OF ELECTRONIC CIRCUIT

1. Oscillator

The purpose of the oscillator is to convert the capacity change of C1 (Fig. B2) to a frequency deviation. The oscillator is comprised of LC tank circuit T1p, C2, R5 and C1, transistor Q1 (Fig. B2) and associated circuitry. The oscillator tank circuit is designed to deviate from 10.6 to 10.9 MHZ when C1 changes over its maximum range of capacity.

This frequency range is chosen because it is one of the input operating frequencies suggested for the demodulator circuit (Fig. B2 Q3).

The collector of oscillator transistor Q1 is tapped into the tank coil T1p ten turns from the decoupled end. This reduces detuning effects of Q1 junction capacity because the latter acts only across a small part of the inductance T1p.

Winding S2 of transformer T1 provides positive feedback to the base of Q1 to sustain oscillation. Resistor R4 and capacitor C3 decouple the oscillator from the 12 VDC power supply.

2. Buffer Amplifier

Buffer amplifier Q2 and associated components (Fig. B2) isolates the input of demodulator Q3 from the oscillator Q1. Winding S1 of transformer T1 couples the oscillator to the buffer amplifier input. Decoupling from the 12 VDC supply is provided by R10 and C4.

3. Demodulator

The demodulator is an integrated circuit which contains a HF limiting amplifier, a quadrature detector and an output amplifier (Fig. B2 Q3). The input signal, conditioned by the limiting amplifier, is coupled to the quadrature detector by C13.

Demodulation is accomplished by comparing the frequency of the conditioned signal to the slope of the band-pass curve of quadrature tank circuit LI, C12 and R16 (Fig. B2).

Capacitor C11 (Fig. B2) in conjunction with an internal 8.8 kΩ resistor provides high frequency roll-off for the demodulated signal. For 10 KHZ response, C11 is calculated to be 0.0018 μF. Resistor R15 and capacitor C14 provide decoupling from the 12 VDC supply.

For detailed information on the demodulator, refer to Motorola specification sheet MC1357.

D. OPERATION

The demodulator and the oscillator buffer amplifier circuitry should be shielded from each other to avoid electro-magnetic coupling between the oscillator LC tank circuit and the quadrature tank circuit (Fig. B1 a and b).

Variable capacitor C2 (Fig. B1a) positions the oscillator frequency within the bandwidth of the demodulator.

Fig. 7 illustrates the relationship between void fraction and output voltage.

BUBBLE DETECTOR PARTS LIST

Resistors (1/nw 5%)

R1	47Ω
R2	47Ω
R3	100Ω
R4	270Ω
R5	33kΩ
R6	18kΩ
R7	2.2kΩ
R8	1kΩ
R9	5.1kΩ
R10	82Ω
R11	100Ω
R12	47Ω
R13	470Ω
R14	47Ω
R15	150Ω
R16	3.9kΩ
R17	560Ω

Capacitors (10%)

C1	4pf
C2	0-100 pF variable
C3	.068
C4	.068
C5	.068
C6	.068
C7	.01
C8	.1
C9	.1
C10	.1
C11	.0018
C12	100 pF
C13	5 pF
C14	.1
C15	.1

Transistors

Q1	=	Motorola MPS 6515
Q2	=	Motorola MPS 6515
Q3	=	Motorola MC 1357 PQ

Coils and Transformers

L1 = 2.3 µH
15 turns, .485" OD

T1:
p = 8.1 µH
47 turns tapped at 10 turns
.452" OD
S1 = 4 turns .452" OD
S2 = 6 turns .452" OD

All windings #24 (AWG) closely wound

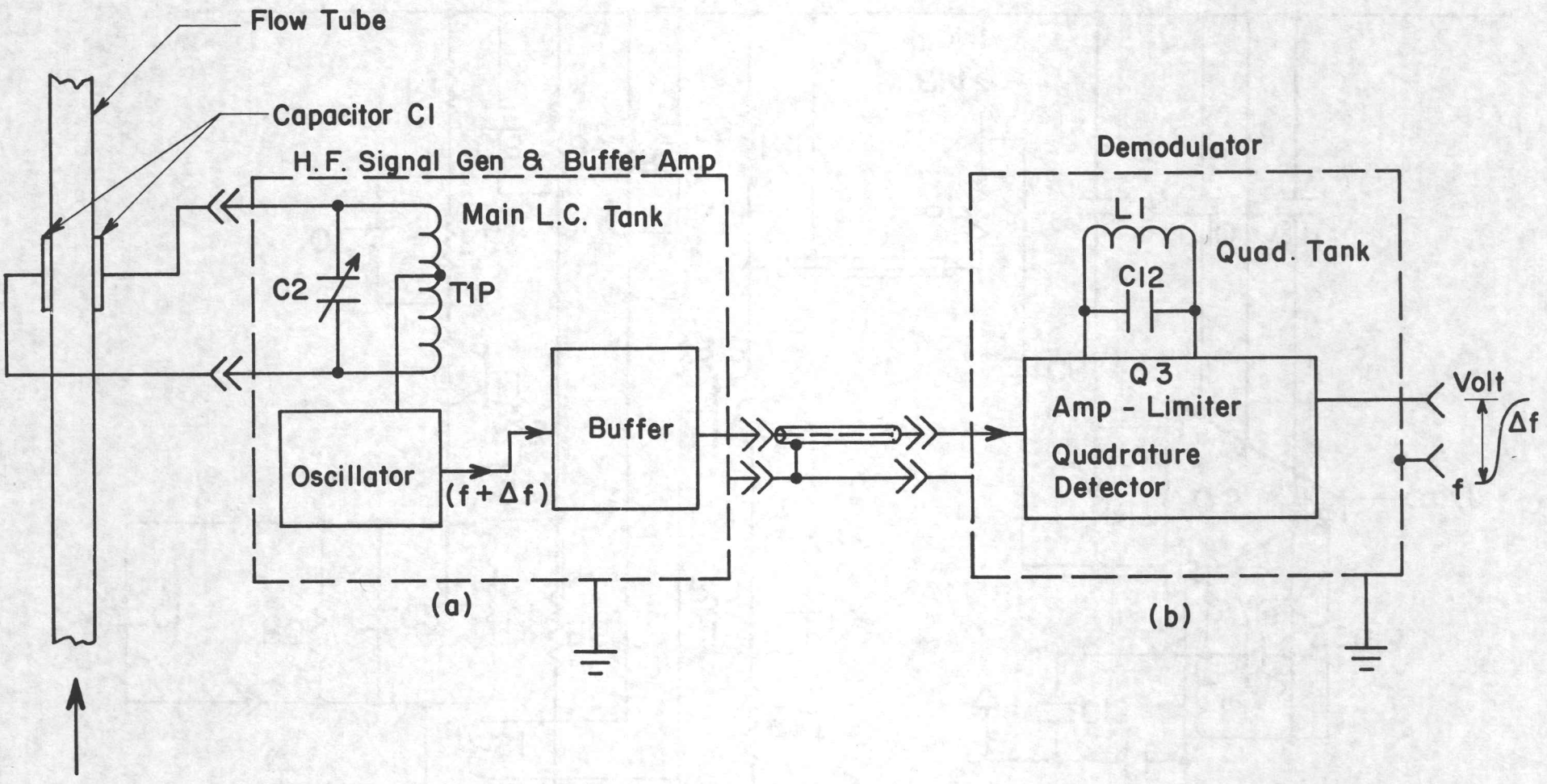

FIG. B1 BUBBLE-DETECTOR ELECTRONICS BLOCK SCHEMATIC

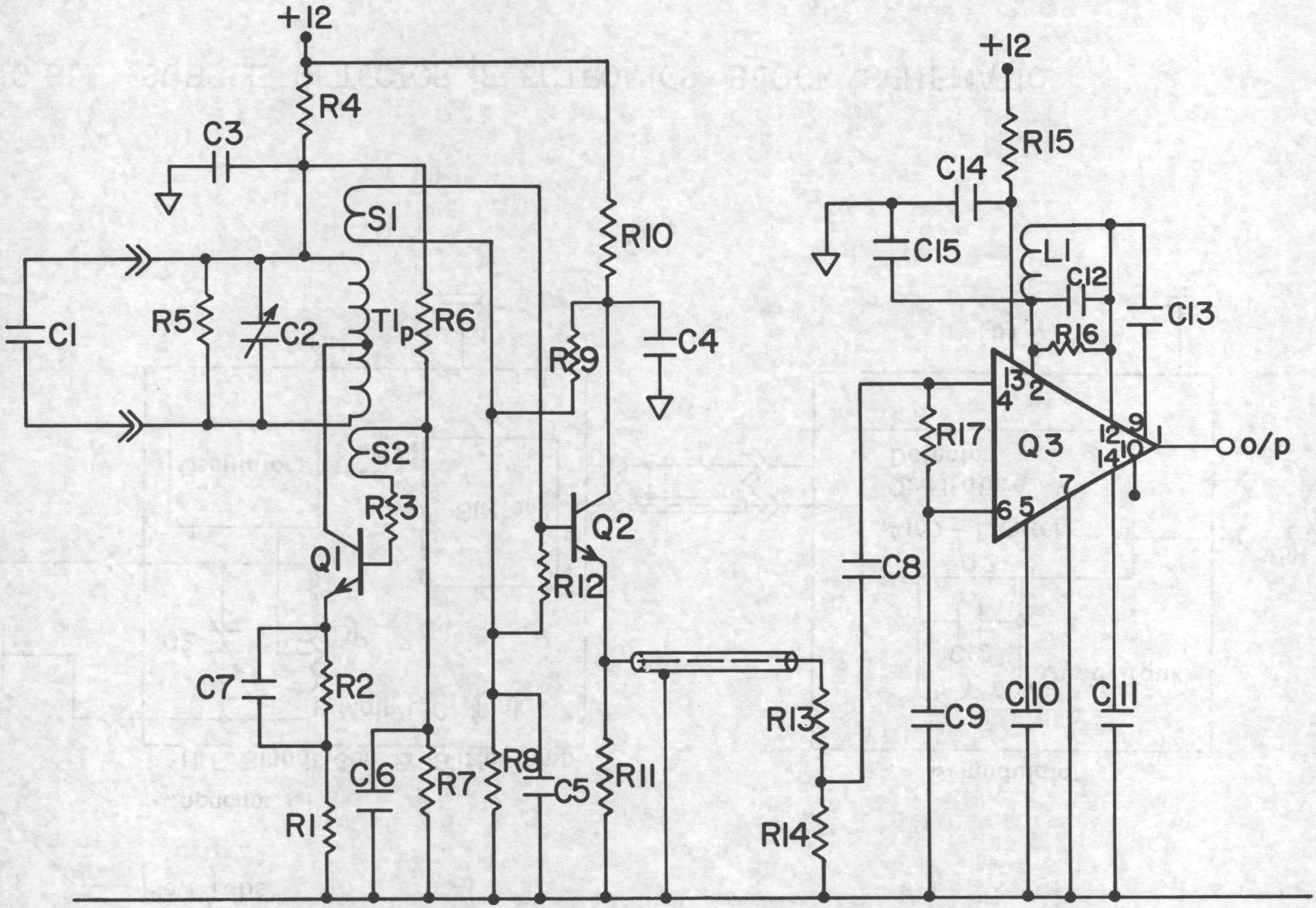

FIG. B2 BUBBLE - DETECTOR SCHEMATIC

UTIAS TECHNICAL NOTE NO. 185

Institute for Aerospace Studies, University of Toronto

VELOCITY MEASUREMENTS IN BUBBLY TWO-PHASE FLOWS USING LASER DOPPLER ANEMOMETRY (PART II)

Davies, W. E. R. and Unger, J. I. 20 pages (approx) 20 figures

1. Laser 2. Anemometry 3. Laser Doppler 4. Flow Measurements
I. Davies, W. E. R. and Unger, J. I. II. UTIAS Technical Note No. 185

The application of the laser Doppler velocity measuring technique to both turbid and bubbly flow media is described. Two types of automatic frequency trackers have been tested and their performance evaluated under a variety of flow conditions. A high frequency void fraction measuring instrument has been developed using a capacity principle and is used to provide information on flow conditions. Full details on the electronics associated with the frequency tracking unit and the void fraction meter are included in the report.

Available copies of this report are limited. Return this card to UTIAS, if you require a copy.

UTIAS TECHNICAL NOTE NO. 185

Institute for Aerospace Studies, University of Toronto

VELOCITY MEASUREMENTS IN BUBBLY TWO-PHASE FLOWS USING LASER DOPPLER ANEMOMETRY (PART II)

Davies, W. E. R. and Unger, J. I. 20 pages (approx) 20 figures

1. Laser 2. Anemometry 3. Laser Doppler 4. Flow Measurements
I. Davies, W. E. R. and Unger, J. I. II. UTIAS Technical Note No. 185

The application of the laser Doppler velocity measuring technique to both turbid and bubbly flow media is described. Two types of automatic frequency trackers have been tested and their performance evaluated under a variety of flow conditions. A high frequency void fraction measuring instrument has been developed using a capacity principle and is used to provide information on flow conditions. Full details on the electronics associated with the frequency tracking unit and the void fraction meter are included in the report.

Available copies of this report are limited. Return this card to UTIAS, if you require a copy.

UTIAS TECHNICAL NOTE NO. 185

Institute for Aerospace Studies, University of Toronto

VELOCITY MEASUREMENTS IN BUBBLY TWO-PHASE FLOWS USING LASER DOPPLER ANEMOMETRY (PART II)

Davies, W. E. R. and Unger, J. I. 20 pages (approx) 20 figures

1. Laser 2. Anemometry 3. Laser Doppler 4. Flow Measurements
I. Davies, W. E. R. and Unger, J. I. II. UTIAS Technical Note No. 185

The application of the laser Doppler velocity measuring technique to both turbid and bubbly flow media is described. Two types of automatic frequency trackers have been tested and their performance evaluated under a variety of flow conditions. A high frequency void fraction measuring instrument has been developed using a capacity principle and is used to provide information on flow conditions. Full details on the electronics associated with the frequency tracking unit and the void fraction meter are included in the report.

Available copies of this report are limited. Return this card to UTIAS, if you require a copy.

UTIAS TECHNICAL NOTE NO. 185

Institute for Aerospace Studies, University of Toronto

VELOCITY MEASUREMENTS IN BUBBLY TWO-PHASE FLOWS USING LASER DOPPLER ANEMOMETRY (PART II)

Davies, W. E. R. and Unger, J. I. 20 pages (approx) 20 figures

1. Laser 2. Anemometry 3. Laser Doppler 4. Flow Measurements
I. Davies, W. E. R. and Unger, J. I. II. UTIAS Technical Note No. 185

The application of the laser Doppler velocity measuring technique to both turbid and bubbly flow media is described. Two types of automatic frequency trackers have been tested and their performance evaluated under a variety of flow conditions. A high frequency void fraction measuring instrument has been developed using a capacity principle and is used to provide information on flow conditions. Full details on the electronics associated with the frequency tracking unit and the void fraction meter are included in the report.

Available copies of this report are limited. Return this card to UTIAS, if you require a copy.